Solid-state supramolecular assembly, luminescence thermometry and solution-state photoisomerization studies in lanthanide polyoxazamacrocycles

Dominika Prętka[a]*, Przemysław Woźny[a], Maciej Kubicki[a], Marcin Runowski[a], Violetta Patroniak[a], Giuseppe Consiglio[b], Giuseppe Forte[c], Adam Gorczyński[a]*

a Faculty of Chemistry, Adam Mickiewicz University in Poznań, Uniwersytetu Poznańskiego 8, 61-614 Poznań, Poland
b Department of Chemical Science University of Catania, Via S. Sofia 64, Italy
c Department of Drug Science and Health University of Catania, Via S. Sofia 64, Italy

Supporting Information

1. Materials and general methods

All organic and inorganic chemicals for the synthesis of macrocyclic ligands, lanthanide salts and solvents were commercially available unless noted otherwise. 2,6-pyridinedicarboxaldehyde was prepared from 2,6-Pyridinedimethanol according to previously reported procedure.[1] Nuclear magnetic resonance spectra were recorded on Bruker Avance Neo (600 MHz) spectrometer and calibrated against the deuterated solvent. Mass spectra were performed on a Waters Micromass ZQ or SQD-2 Spectrometers. Simulations of mass spectra were conducted with enviPat programme.[2] FT-IR spectra were conducted with a Bruker FT-IR IFS 66/s spectrophotometer and peak positions are reported in cm^{-1}. Powder X-ray diffraction (PXRD) analyses were performed using a Bruker AXS D8 Advance diffractometer in a quartz zero-background plate. Thermogravimetry (TG) analysis was conducted on Netzsch TG 209 Libra analyser under N_2 atmosphere in the temperature range of ~25–1000°C. Photoisomerization studies were performed for all samples in chloroform solution ($c = 2.0 \times 10^{-5}$ M). Light irradiation at different wavelengths was performed using the Tunable Light Source consists of a Broadband Light Source, 150W Xenon Light Source and a MO250 Monochromator (OPTEL Opole). The light intensity during irradiation was monitored and controlled using a radiometer to maintain stable conditions. The radiometer with a range up to $10mW/cm^2$ with resolution of $0.01mW/cm^2$ was used as a light power meter (OPTEL Opole). Precision bandwidth is < 1 nm based on the grating with a density of 600 lines/mm. All calculations were performed using a multilevel computational protocol combining conformational sampling and density functional theory (DFT) optimization. The conformational landscape of the macrocyclic scaffold was first explored using the CREST conformer–rotamer ensemble sampling tool in combination with the GFN2-xTB semiempirical Hamiltonian.[3] This approach allows an efficient exploration of multidimensional potential energy surfaces and has proven particularly effective for flexible molecular systems with large conformational freedom. Implicit solvation corresponding to chloroform was included during the sampling procedure. For each protonation state of the ligand (neutral, protonated, and deprotonated), CREST generated a large ensemble of conformers that were subsequently ranked according to their relative energies. The resulting ensembles were analyzed in terms of energy distributions and cumulative energy profiles, allowing a quantitative evaluation of the density of low-lying minima in the potential energy surface. Such computational strategies, combining geometry optimization and analysis of intermolecular interactions to elucidate structural stability and energetic landscapes, are widely employed in molecular modeling studies of complex systems. For example, force-field based geometry optimization and molecular simulations have been successfully used to analyze molecular interaction landscapes and structural stability in surface–molecule systems.[4] From the CREST ensembles, the lowest-energy structures were inspected and representative conformers were selected based on structural diversity and relative energy. For each protonation state, five representative conformers were retained for further quantum mechanical refinement. Selected conformers were subsequently optimized using density functional theory. Geometry optimizations and frequency calculations were performed using Gaussian 16.[5] The optimized structures were confirmed as true minima by vibrational frequency analysis (no imaginary frequencies). Gibbs free energies were computed at 298 K and used to determine relative conformer stability. The relative Gibbs free energies were then used to construct energy ladder diagrams illustrating the thermodynamic accessibility of the refined conformational minima.

2. Experimental section

2.1. Detailed synthetic procedures and characterization

Representation of studied macrocyclic ligands

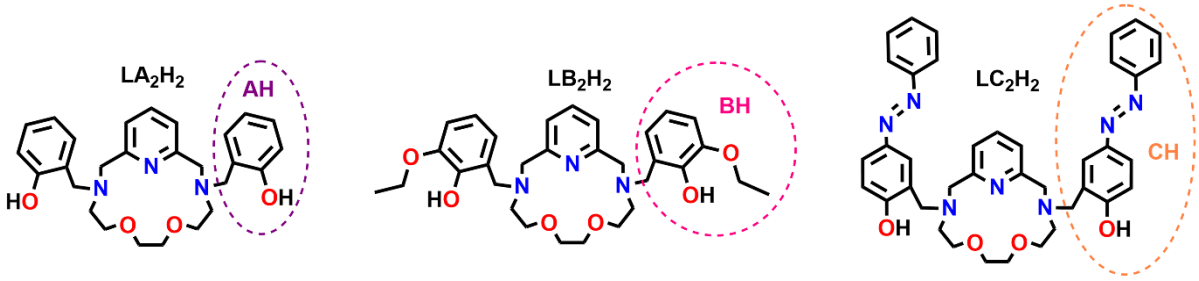

2.1.1. Synthesis of ligands and its protonated salt (Figures S1-S8)

Synthesis of ligand **LA_2H_2**

Macrocyclic precursor **LH_2** (0.50 g, 1.99 mmol) was dissolved in tetrahydrofuran (60 ml) in 100 ml round-bottom flask. Then salicylaldehyde (0.51 g, 4.18 mmol), acetic acid (0.24 ml, 4.18 mmol) and sodium triacetoxyborohydride (2.07 g, 9.77 mmol) were added. The reaction mixture was heated at 60°C for 48 hours with continuous stirring. A saturated solution of potassium hydrogen carbonate was added until the pH reached approximately 8. The organic layer was separated and dried over anhydrous sodium sulphate. Then the solvent was evaporated to dryness. The oily residue was dissolved in chloroform, and the solution was passed through a very short column of neutral alumina. Collected fractions were evaporated to dryness. Acetonitrile was added to the yellow oily residue, and a recrystallization process was carried out. The white precipitate was separated from solution by filtration and washed three times with diethyl ether. The product was dried under vacuum to give a white powder in 66% yield (0.61 g), based on the precursor **LH_2**.

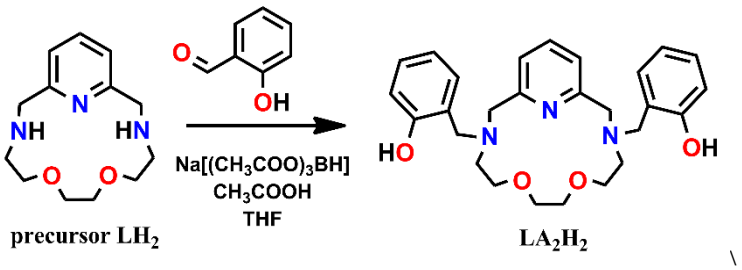

Fig. S1. Synthesis scheme for ligand **LA_2H_2**.

^{1}H NMR (600 MHz, DMSO-d_6) δ 10.30 (s, 2H), 7.71 (t, *J* = 7.6 Hz, 1H), 7.18 (d, *J* = 7.6 Hz, 2H), 7.16 (dd, *J* = 7.8, 1.6 Hz, 2H), 7.11 (td, *J* = 7.7, 1.7 Hz, 2H), 6.76 (t, *J* = 7.2 Hz, 4H), 3.83 (s, 4H), 3.73 (s, 4H), 3.44 (t, *J* = 6.1 Hz, 4H), 3.32 (s, 4H), 2.69 (t, *J* = 6.1 Hz, 4H).

^{13}C NMR (151 MHz, DMSO-d_6) δ 157.48, 157.17, 136.87, 129.32, 128.33, 123.42, 122.13, 118.75, 115.67, 69.94, 67.63, 59.55, 57.46, 53.05.

ESI-MS(+) m/z = 274 [**LH_2**+Na]$^+$ (calc. for [$C_{13}H_{21}N_3O_2Na$]$^+$: 274.15; 380 [**LHAH**+Na]$^+$ (calc. for [$C_{20}H_{27}N_3O_3Na$]$^+$: 380.20); 486 [**LA_2H_2**+Na]$^+$ (calc. for [$C_{27}H_{33}N_3O_4Na$]$^+$: 486.24).

Selected IR (KBr, cm^{-1}): ν(O-H)$_{phenol}$ 3413, ν(C-H)$_{ar}$ 3047, ν(C-H) 2942-2846, ν(C=C), ν(C=N) 1610, 1587, 1489, 1476, 1452, 1384, 1356, 1308, ν(C-N) 1255, ν(C-O) 1128.

Ligand **LA_2** in its sodium salt form Na**LA_2H**(CH_3OH)

As an initial study, the ligand was synthesized under the same reaction conditions, but an aqueous solution of sodium hydroxide (instead of potassium hydrogen carbonate) was used to obtain alkaline conditions. Under these conditions (pH higher than 8), the ligand was isolated in the form of its sodium salt. Single crystals suitable for X-ray analysis were obtained by recrystallization from a solution of ethyl acetate and methanol. This method was not further used, as our goal was to isolate ligand in its free form, as described above, to facilitate complexation with lanthanides and avoid competition between sodium and lanthanide ions.

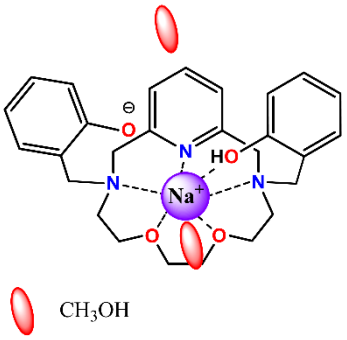

Fig. S2. Schematic representation of the Na**LA_2H**(CH_3OH) compound.

Synthesis of ligand **LB_2H_2**

Macrocyclic precursor **LH_2** (0.50 g, 1.99 mmol) was dissolved in tetrahydrofuran (60 ml) in 100 ml round-bottom flask. Then 3-ethoxysalicylaldehyde (0.69 g, 4.18 mmol), acetic acid (0.24 ml, 4.18 mmol) and sodium triacetoxyborohydride (2.07 g, 9.77 mmol) were added. The reaction mixture was heated at 60°C for 48 hours with continuous stirring. A saturated solution of potassium hydrogen carbonate was added until the pH reached approximately 8. The organic layer was separated and dried over anhydrous sodium sulphate. Then the solvent was evaporated to dryness. The oily residue was dissolved in chloroform, and the solution was passed through a very short column of neutral alumina. Collected fractions were evaporated to dryness. Acetonitrile was added to the yellow oily residue, and a recrystallization process was carried out. The white precipitate was separated from solution by filtration and washed three times with diethyl ether. The product was dried under vacuum to give a white powder in 51% yield (0.56 g), based on the precursor **LH_2**. Single crystals suitable for X-ray analysis were obtained by slow evaporation from acetonitrile solution.

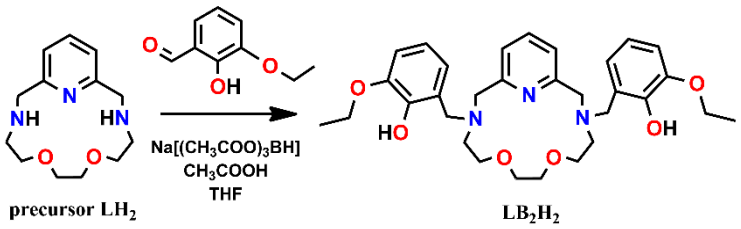

Fig. S3. Synthesis scheme for ligand **LB_2H_2.**

^{1}H NMR (600 MHz, Methylene Chloride-d_2) δ 10.51 (s, 2H), 7.61 (t, *J* = 7.6 Hz, 1H), 7.12 (d, *J* = 7.6 Hz, 2H), 6.82 (dd, *J* = 7.9, 1.6 Hz, 2H), 6.71 (t, *J* = 7.7 Hz, 2H), 6.67 (dd, *J* = 7.6, 1.6 Hz, 2H), 4.06 (q, *J* = 7.0 Hz, 4H), 3.88 (s, 4H), 3.80 (s, 4H), 3.56 (t, *J* = 6.0 Hz, 4H), 3.44 (s, 4H), 2.83 (t, *J* = 6.0 Hz, 4H), 1.43 (t, *J* = 7.0 Hz, 6H).

^{13}C NMR (151 MHz, Methylene Chloride-d_2) δ 157.91, 148.32, 147.88, 137.17, 123.82, 122.74, 121.67, 118.86, 113.98, 71.12, 68.45, 64.92, 60.51, 59.71, 54.06, 15.31.

ESI-MS(+) m/z = 252 [**LH_2**+H]$^+$ (calc. for $[C_{13}H_{22}N_3O_2]^+$: 252.17; 402 [**LHBH**+H]$^+$ (calc. for $[C_{22}H_{32}N_3O_4]^+$: 402.24); 552 [**LB_2H_2** +H]$^+$ (calc. for $[C_{31}H_{42}N_3O_6]^+$: 552.31); 574 [**LB_2H_2** +Na]$^+$ (calc. for $[C_{31}H_{41}N_3O_6Na]^+$: 574.29).

Selected IR (KBr, cm^{-1}): ν(O-H)$_{phenol}$ 3430, ν(C-H)$_{ar}$ 3046, ν(C-H) 2982-2817, ν(C=C), ν(C=N) 1584, 1490, 1474, 1441, 1388, 1369, 1307, ν(C-N) 1238, ν(C-O) 1115.

Synthesis of ligand **LC_2H_2**

Macrocyclic precursor **LH_2** (0.50 g, 1.99 mmol), 4-phenylazaphenol (1.00 g, 5 mmol) and paraformaldehyde (0.15 g, 5 mmol) were placed in the 250 ml two-necked round-bottom flask. Under inert atmosphere 100 ml of anhydrous toluene was introduced. The reaction mixture was heated at reflux conditions for 24 hours with continuous stirring. The solvent was removed under reduced pressure, and the oily dark-red residue was purified by column chromatography (SiO_2, methanol:dichloromethane; 95:5). Fractions with product were collected and evaporated to dryness to obtain red oil. The product was obtained in the form of orange crystalline material by slow evaporation from acetone. Obtained crystalline powder was dried under vacuum to give a product in 40% yield (0.54 g), based on the precursor **LH_2**.

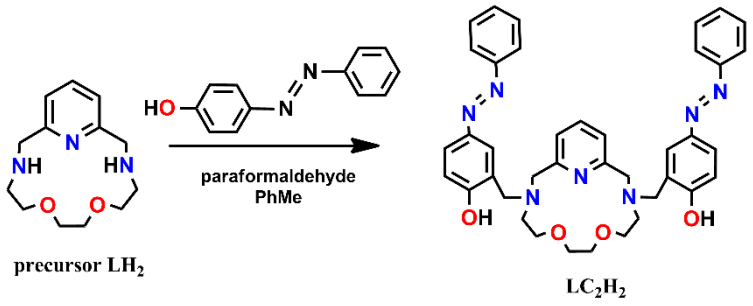

Fig. S4. Synthesis scheme for ligand **LC_2H_2.**

^{1}H NMR (600 MHz, Chloroform-*d*) δ 7.87 – 7.83 (m, 6H), 7.70 (d, *J* = 2.4 Hz, 2H), 7.58 (t, *J* = 7.6 Hz, 1H), 7.51 – 7.48 (m, 4H), 7.44 – 7.40 (m, 2H), 7.09 (d, *J* = 7.6 Hz, 2H), 6.97 (d, *J* = 8.6 Hz, 2H), 3.99 (s, 4H), 3.89 (s, 4H), 3.67 (t, *J* = 5.8 Hz, 4H), 3.53 (s, 4H), 2.92 (t, *J* = 5.7 Hz, 4H).

^{13}C NMR (151 MHz, Chloroform-*d*) δ 161.61, 157.35, 153.01, 146.00, 137.11, 130.24, 129.16, 125.39, 123.42, 123.13, 122.61, 122.56, 117.22, 70.95, 68.17, 60.15, 59.27, 53.91.

ESI-MS(+) m/z = 252 [**LH_2**+H]$^+$ (calc. for $[C_{13}H_{22}N_3O_2]^+$: 252.17); 462 [**LHCH+**H]$^+$ (calc. for $[C_{26}H_{32}N_5O_3]^+$: 462.25); 672 [**LC_2H_2** +H]$^+$ (calc. for $[C_{39}H_{42}N_7O_4]^+$: 672.33).

Selected IR (KBr, cm^{-1}): ν(O-H)$_{phenol}$ 3436, ν(C-H)$_{ar}$ 3064, ν(C-H) 2909-2859, ν(C=C), ν(C=N) 1589, 1587, 1476, 1455, 1443, 1430, 1384, 1356, 1308, ν(N=N) 1489, ν(C-N) 1255, ν(C-O) 1179.

Protonated form of ligand **LC_2H_2** as its hydrochloride salt **$LH_2^{2+}C_2H_2{\cdot}2Cl^-$**

As a preliminary result, purification of the ligand after removal of toluene, was carried out by acid-base extraction in a mixture of dichloromethane and water, using hydrochloric acid and sodium hydroxide to control the pH conditions. After extraction, an orange solid precipitated from the aqueous phase. Single crystals for X-ray analysis were obtained by slow diffusion of diethyl ether into the methanolic solution of obtained powder. Resolved structure indicated a high affinity for protonation of the ligand (nitrogen atoms), and formation of the compound as its chloride salt. Tests of the complexation reactions with lanthanide salts confirmed (as described in detail below) that it is no possibility to coordinate the lanthanide ion by the protonated macrocycle system. Therefore, the synthesis of the ligand described above (synthesis of ligand **LC_2H_2**) was chosen as the synthesis method and used further successfully for the formation of lanthanide complexes.

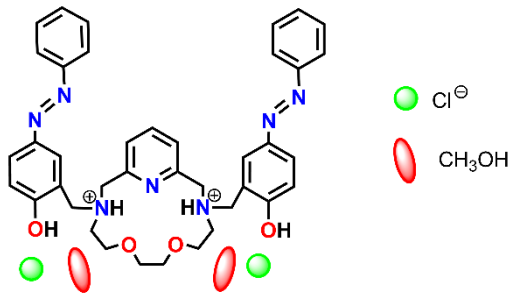

Fig. S5. Schematic representation of the **$LH_2^{2+}C_2H_2{\cdot}2Cl^-$** compound.

Protonated form of ligand **LC_2H_2** as its triflate salt **$LH_2^{2+}C_2H_2{\cdot}2CF_3SO_3^-$**

Single crystals for X-ray analysis were obtained by slow diffusion of diisopropyl ether into the acetonitrile:dichlorometane (2:1) solution, when approaches were undertaken to complexate the **$LH_2^{2+}C_2H_2{\cdot}2Cl^-$** protonated ligand salt with lanthanide triflate.

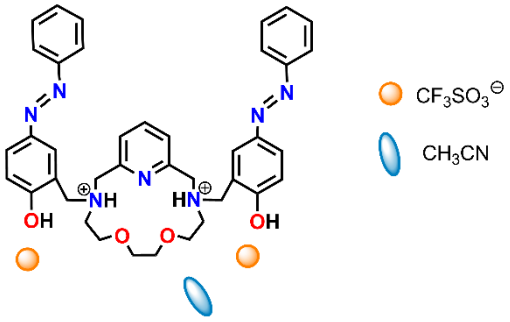

Fig. S6. Schematic representation of the $LH_2^{2+}C_2H_2 \cdot 2CF_3SO_3^-$ compound.

Protonated form of ligand LB_2H_2 as its oxalate salt $LH_2^{2+}B_2H_2 \cdot 2HC_2O_4^-$

Single crystals for X-ray analysis were obtained by slow diffusion of diisopropyl ether into the methanol:acetone (1:1) solution, when approaches were undertaken to complexate the LB_2H_2 ligand with lanthanide triflate in the presence of oxalic acid.

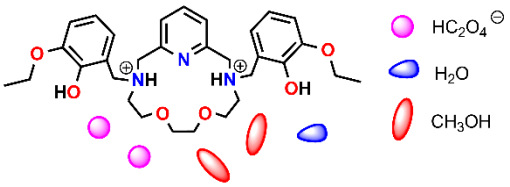

Fig. S7. Schematic representation of the $LH_2^{2+}B_2H_2 \cdot 2HC_2O_4^-$ compound.

Protonated form of ligand LB_2H_2 as its triflate salt $LH_2^{2+}B_2H_2 \cdot 2CF_3SO_3^-$

Single crystals suitable for X-ray analysis were obtained by slow diffusion of diisopropyl ether into the acetonitrile:dichlorometane (2:1) solution, when approaches were undertaken to complexate the $LH_2^{2+}B_2H_2 \cdot 2HC_2O_4^-$ protonated ligand salt form with lanthanide triflate.

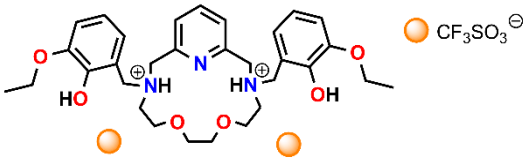

Fig. S8. Schematic representation of the $LH_2^{2+}B_2H_2 \cdot 2CF_3SO_3^-$ compound.

2.1.2. Synthesis of Ln-macrocyclic complexes

Synthesis of Dy/LA_2 lanthanide complex

Ligand LA_2H_2 (50.00 mg, 0.11 mmol) was placed in the 50 ml round-bottom flask, followed by the addition of 20 ml of acetonitrile and triethylamine (30.00 µl, 0.22 mmol). $Dy(CF_3SO_3)_3$ (65.76 mg, 0.11 mmol) was then added, with a visible colour change of the solution to light yellow. The resulting mixture was stirred at 80°C for 24 hours. The solvent was then removed under reduced pressure to a minimal amount (1 ml) and excess of diethyl ether

was added. The precipitated solid was filtered, washed with diethyl ether and dried under vacuum to give 60.11 mg of the product as a white powder. Single crystals suitable for X-ray analysis were obtained for monometallic 1+1 assembly by slow diffusion of diisopropyl ether into the acetonitrile:methanol (1:1) solution - Dy**LA$_2$**(H_2O) complex.

ESI-MS(+) m/z = 625 [Dy**LA$_2$**]$^+$ (calc. for [$C_{27}H_{31}N_3O_4Dy$]$^+$: 625.16); 1397 [(Dy**LA$_2$**)$_2$+CF_3SO_3]$^+$ (calc. for [$C_{55}H_{62}F_3N_6O_{11}SDy_2$]$^+$: 1397.27).

Selected IR (KBr, cm^{-1}): ν(O-H)$_{MeOH,\ water}$ 3396, ν(C-H)$_{ar}$ 3062, ν(C-H) 2982-2850, ν(C=C), ν(C=N) 1609, 1596, 1482, 1454, $\nu_{as}(SO_3)$ 1274, $\nu_{as}(CF_3)$ 1258, 1224, $\nu_s(CF_3)$ 1164, $\nu_s(SO_3)$ 1030, ν(Ln-O) 639.

Synthesis of Nd/**LA$_2$** lanthanide complex

Ligand **LA$_2$H$_2$** (50.00 mg, 0.11 mmol) was placed in the 50 ml round-bottom flask, followed by the addition of 20 ml of acetonitrile and triethylamine (30.00 µl, 0.22 mmol). $Nd(CF_3SO_3)_3$ (63.79 mg, 0.11 mmol) was then added, with a visible colour change of the solution to light yellow. The resulting mixture was stirred at 80^{o}C for 24 hours. The solvent was then removed under reduced pressure to a minimal amount (1 ml) and excess of diethyl ether was added. The precipitated solid was filtered, washed with diethyl ether and dried under vacuum to give 54.62 mg of the product as a white powder. Single crystals suitable for X-ray analysis were obtained for dimetallic 2+2 assembly by slow diffusion of diisopropyl ether into the acetonitrile:methanol (1:1) solution - Nd_2(**LA$_2$**)$_2$(H_2O)$_2$ complex.

ESI-MS(+) m/z = 605 [Nd**LA$_2$**]$^+$ (calc. for [$C_{27}H_{31}N_3O_4Nd$]$^+$: 605.14); 1360 [(Nd**LA$_2$**)$_2$+CF_3SO_3]$^+$ (calc. for [$C_{55}H_{62}F_3N_6O_{11}SNd_2$]$^+$: 1359.24).

Selected IR (KBr, cm^{-1}): ν(O-H) $_{MeOH,\ water}$ 3476, ν(C-H)$_{ar}$ 3062, ν(C-H) 2943-2844, ν(C=C), ν(C=N) 1596, 1579, 1480,1454, $\nu_{as}(SO_3)$ 1279, $\nu_{as}(CF_3)$ 1261, 1223, $\nu_s(CF_3)$ 1162, $\nu_s(SO_3)$ 1030, ν(Ln-O) 638.

Synthesis of La/**LB$_2$** lanthanide complex

Ligand **LB$_2$H$_2$** (21.00 mg, 0.04 mmol) was placed in the 25 ml round-bottom flask, followed by the addition of 10 ml of acetonitrile and triethylamine (10.6 µl, 0.08 mmol). $La(CF_3SO_3)_3$ (22.31 mg, 0.04 mmol) was then added. The resulting mixture was stirred at 80^{o}C for 24 hours. The solvent was then removed under reduced pressure to a minimal amount (1 ml) and excess of diethyl ether was added. The precipitated solid was filtered, washed with diethyl ether and dried under vacuum to give 25.00 mg of the product as a white powder.

ESI-MS(+) m/z = 688 [La**LB$_2$**]$^+$ (calc. for [$C_{31}H_{39}N_3O_6La$]$^+$: 688.19); 1525 [(La**LB$_2$**)$_2$+CF_3SO_3]$^+$ (calc. for [$C_{63}H_{78}F_3N_6O_{15}SLa_2$]$^+$: 1525.33).

Synthesis of La/**LB$_2$**(urea) lanthanide complex

Ligand **LB$_2$H$_2$** (21.00 mg, 0.04 mmol) was placed in the 25 ml round-bottom flask, followed by the addition of 10 ml of acetonitrile and triethylamine (10.6 µl, 0.08 mmol). $La(CF_3SO_3)_3$ (22.31 mg, 0.04 mmol) and urea (2.29 mg, 0.04 mmol) were then added. The resulting mixture was stirred at 80^{o}C for 24 hours. The solvent was then

removed under reduced pressure to a minimal amount (1 ml) and excess of diethyl ether was added. The precipitated solid was filtered, washed with diethyl ether and dried under vacuum to give 29.13 mg of the product as a white powder.

ESI-MS(+) m/z = 688 [La**LB$_2$**]$^+$ (calc. for [$C_{31}H_{39}N_3O_6La$]$^+$: 688.19); 748 [La**LB$_2$**+$CO(NH_2)_2$]$^+$ (calc. for [$C_{32}H_{43}N_5O_7La$]$^+$: 748.22); 1525 [(La**LB$_2$**)$_2$+CF_3SO_3]$^+$ (calc. for [$C_{63}H_{78}F_3N_6O_{15}SLa_2$]$^+$: 1525.33).

Synthesis of Dy/**LB$_2$** lanthanide complexes

Ligand **LB$_2$H$_2$** (50.00 mg, 0.09 mmol) was placed in the 50 ml round-bottom flask, followed by the addition of 20 ml of acetonitrile and triethylamine (25.3 µl, 0.18 mmol). $Dy(CF_3SO_3)_3$ (55.26 mg, 0.09 mmol) was then added, with a visible colour change of the solution to light yellow. The resulting mixture was stirred at 80^{o}C for 24 hours. The solvent was then removed under reduced pressure to a minimal amount (1 ml) and excess of diethyl ether was added, which resulted in the formation of an oily product. Although, there were difficulties in obtaining product in the solid state, diethyl ether and acetonitrile was removed under reduced pressure, DMSO (10 ml) was added to the oily yellow residue, and several monocrystals were obtained directly from this solution after slow evaporation - Dy**LB$_2$**(DMSO) complex.

ESI-MS(+) m/z = 713 [Dy**LB$_2$**]$^+$ (calc. for [$C_{31}H_{39}N_3O_6Dy$]$^+$: 713.21); 885 [Dy**LB$_2$**+Na+CF_3SO_3]$^+$ (calc. for [$C_{32}H_{39}F_3N_3O_9SNaDy$]$^+$: 885.15); 1573 [(Dy**LB$_2$**)$_2$+$CF_3SO_3$]$^+$ (calc. for [$C_{63}H_{78}F_3N_6O_{15}SDy_2$]$^+$: 1573.38).

Dy/**LB$_2$** complex: Ligand **LB$_2$H$_2$** (0.09 mmol) was placed in the 50 ml round-bottom flask, followed by the addition of 20 ml of acetonitrile and triethylamine (25.3 µl, 0.18 mmol). $Dy(CF_3SO_3)_3$ (55.26 mg, 0.09 mmol) and urea (5.44 mg, 0.09 mmol) were then added, with a visible colour change of the solution to light yellow. The resulting mixture was stirred at 80^{o}C for 24 hours. The product was crystalized directly from the reaction mixture by slow diffusion of diisopropyl ether into the acetonitrile solution. Obtained white crystals were filtered, washed with diisopropyl ether and dried under vacuum to give 58.52 mg of the product. Single crystals obtained directly from the reaction mixture were suitable for X-ray analysis and resolved as monometallic 1+1 assembly - Dy**LB$_2$**(urea) complex. This complex was also obtained in a powder form. After evaporation the reaction mixture to a minimal amount (1 ml), excess of diethyl ether was added. The precipitated solid was filtered, washed with diethyl ether and dried under vacuum to give 66.50 mg of the product as a white powder.

ESI-MS(+) m/z = 713 [Dy**LB$_2$**]$^+$ (calc. for [$C_{31}H_{39}N_3O_6Dy$]$^+$: 713.21); 773 [Dy**LB$_2$**+$CO(NH_2)_2$]$^+$ (calc. for [$C_{32}H_{43}N_5O_7Dy$]$^+$: 773.25); 1573 [(Dy**LB$_2$**)$_2$+CF_3SO_3]$^+$ (calc. for [$C_{63}H_{78}F_3N_6O_{15}SDy_2$]$^+$: 1573.38).

Selected IR (KBr, cm^{-1}): $\nu(NH_2)$ 3416, ν(C-H)$_{ar}$ 3231, 3178, ν(C-H) 2978-2893, ν(C=O) 1652, ν(C=C), ν(C=N) 1607, 1592, 1475, 1394, $\nu_{as}(SO_3)$ 1284, $\nu_{as}(CF_3)$ 1255, 1235, $\nu_s(CF_3)$ 1161, $\nu_s(SO_3)$ 1030, ν(Ln-O) 638.

Synthesis of Nd/**LB$_2$** lanthanide complex

Ligand **LB$_2$H$_2$** (50.00 mg, 0.09 mmol) was placed in the 50 ml round-bottom flask, followed by the addition of 20 ml of acetonitrile and triethylamine (25.3 µl, 0.18 mmol). $Nd(CF_3SO_3)_3$ (53.60 mg, 0.09 mmol) and urea (5.44 mg, 0.09 mmol) were then added, with a visible colour change of the solution to light yellow. The resulting mixture

was stirred at 80°C for 24 hours. The product was crystalized directly form the reaction mixture by slow diffusion of diisopropyl ether into the acetonitrile solution. Obtained off-white crystals were filtered, washed with diisopropyl ether and dried under vacuum to give 52.45 mg of the product. Single crystals obtained directly from the reaction mixture were suitable for X-ray analysis and resolved as monometallic 1+1 assembly - Nd**LB$_2$**(urea) complex.

ESI-MS(+) m/z = 691 [Nd**LB$_2$**]$^+$ (calc. for [$C_{31}H_{39}N_3O_6Nd$]$^+$: 691.19); 753 [Nd**LB$_2$**+$CO(NH_2)_2$]$^+$ (calc. for [$C_{32}H_{43}N_5O_7Nd$]$^+$: 753.23); 1535 [(Nd**LB$_2$**)$_2$+CF_3SO_3]$^+$ (calc. for [$C_{63}H_{78}F_3N_6O_{15}SNd_2$]$^+$: 1535.34).

Selected IR (KBr, cm^{-1}): $\nu(NH_2)$ 3442, ν(C-H)$_{ar}$ 3244, 3079, ν(C-H) 2985-2897, ν(C=O) 1663, ν(C=C), ν(C=N) 1634, 1598, 1474, 1383, $\nu_{as}(SO_3)$ 1279, $\nu_{as}(CF_3)$ 1253, 1225, $\nu_s(CF_3)$ 1164, $\nu_s(SO_3)$ 1029, ν(Ln-O) 638.

Synthesis of Dy/**LC$_2$** lanthanide complex

Ligand **LC$_2$H$_2$** (50.00 mg, 0.07 mmol) was placed in the 50 ml round-bottom flask, followed by the addition of 20 ml of acetonitrile and triethylamine (20.70 µl, 0.14 mmol). $Dy(CF_3SO_3)_3$ (45.38 mg, 0.07 mmol) was then added, with a visible colour change of the solution to orange. The resulting mixture was stirred at 80°C for 24 hours. The solvent was then removed under reduced pressure to a minimal amount (1 ml) and excess of diethyl ether was added. The precipitated solid was filtered, washed with diethyl ether and dried under vacuum to give 52.64 mg of the product as an orange powder. Single crystals suitable for X-ray analysis were obtained for monometallic 1+1 and dimetallic 2+2 assembly, under the same conditions - by slow diffusion of diisopropyl ether into the acetonitrile:dichloromethane (2:1) solution - Dy**LC$_2$**(H_2O) and Dy_2(**LC$_2$**)$_2$(OH^-) complexes.

ESI-MS(+) m/z = 833 [Dy**LC$_2$**]$^+$ (calc. for [$C_{39}H_{39}N_7O_4Dy$]$^+$: 833.24); 1814 [(Dy**LC$_2$**)$_2$+CF_3SO_3]$^+$ (calc. for [$C_{79}H_{78}F_3N_{14}O_{11}SDy_2$]$^+$: 1813.42).

Selected IR (KBr, cm^{-1}): ν(O-H)$_{water}$ 3404, ν(C-H)$_{ar}$ 3062, ν(C-H) 2982-2850, ν(C=C) ν(C=N) 1592, 1550, 1444, 1416, ν(N=N) 1482, $\nu_{as}(SO_3)$ 1290, $\nu_{as}(CF_3)$ 1248, 1223, $\nu_s(CF_3)$ 1184, $\nu_s(SO_3)$ 1029, ν(Ln-O) 638.

Synthesis of Nd/**LC$_2$** lanthanide complex

Ligand **LC$_2$H$_2$** (50.00 mg, 0.07 mmol) was placed in the 50 ml round-bottom flask, followed by the addition of 20 ml of acetonitrile and triethylamine (20.70 µl, 0.14 mmol). $Nd(CF_3SO_3)_3$ (44.02 mg, 0.07 mmol) was then added, with a visible colour change of the solution to red. The resulting mixture was stirred at 80°C for 24 hours. The solvent was then removed under reduced pressure to a minimal amount (1 ml) and excess of diethyl ether was added. The precipitated solid was filtered, washed with diethyl ether and dried under vacuum to give 48.80 mg of the product as a red powder. Single crystals suitable for X-ray analysis were obtained for dimetallic 2+2 assembly by slow diffusion of diisopropyl ether into the acetonitrile:dichloromethane (2:1) solution - Nd_2(**LC$_2$**)$_2$(OH^-) complex.

ESI-MS(+) m/z = 813 [Nd**LC$_2$**]$^+$ (calc. for [$C_{39}H_{39}N_7O_4Nd$]$^+$: 813.22).

Selected IR (KBr, cm^{-1}): ν(O-H)$_{water}$ 3396, ν(C-H)$_{ar}$ 3058, ν(C-H) 2953-2847, ν(C=C), ν(C=N) 1593, 1440, 1412, ν(N=N) 1481, $\nu_{as}(SO_3)$ 1291,, $\nu_{as}(CF_3)$ 1258, 1223, $\nu_s(CF_3)$ 1181, $\nu_s(SO_3)$ 1029, ν(Ln-O) 638.

2.1.3. NMR spectroscopy of macrocyclic ligands (Figures S9-S14)

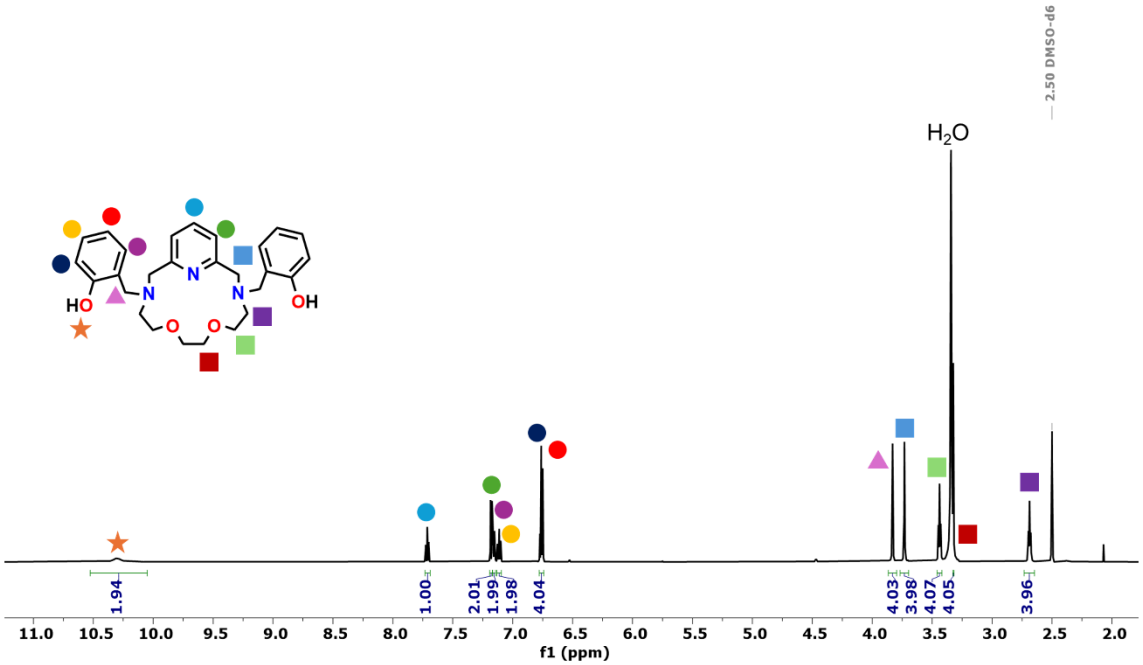

Fig. S9. ^{1}H NMR (600 MHz) spectrum of $\mathbf{LA_2H_2}$ ligand in DMSO-*d6*.

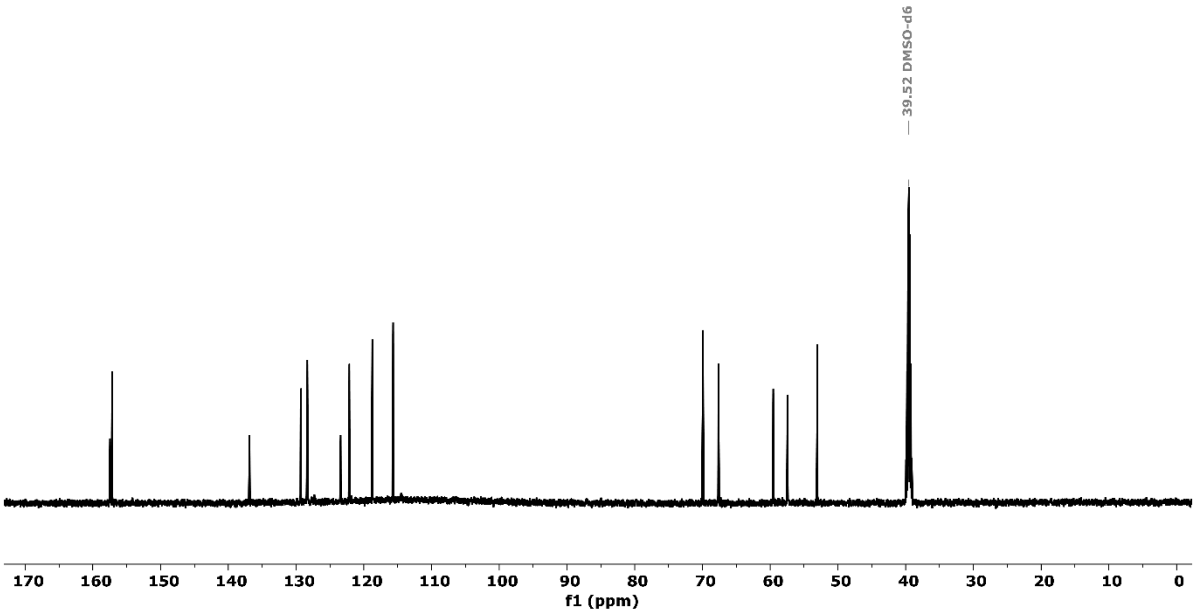

Fig. S10. ^{13}C NMR (151 MHz) spectrum of $\mathbf{LA_2H_2}$ ligand in DMSO-*d6*.

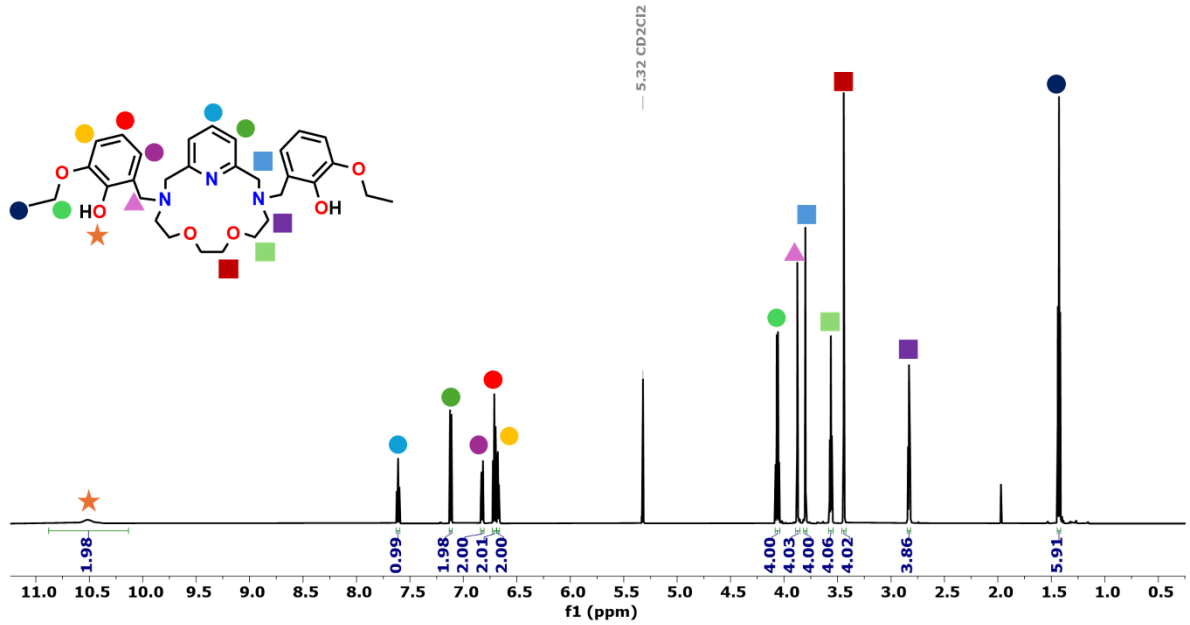

Fig. S11. ^{1}H NMR (600 MHz) spectrum of **LB_2H_2** ligand in CD_2Cl_2.

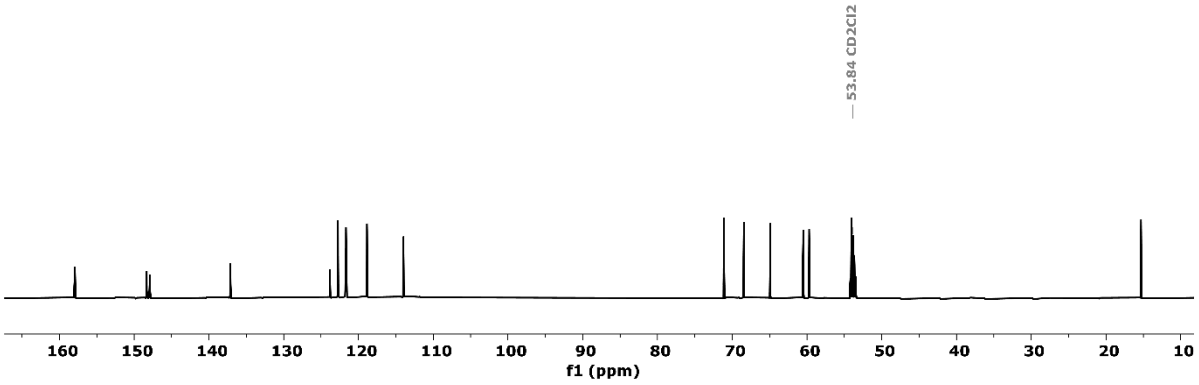

Fig. S12. ^{13}C NMR (151 MHz) spectrum of **LB_2H_2** ligand in CD_2Cl_2.

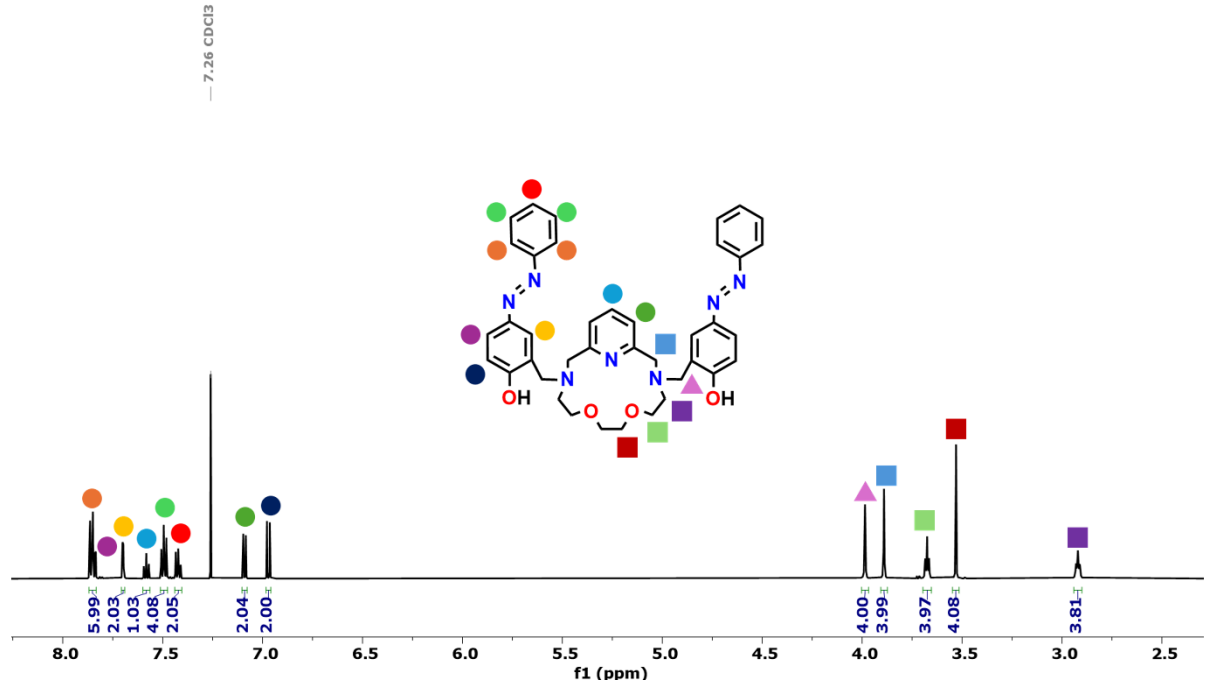

Fig. S13. ^{1}H NMR (600 MHz) spectrum of **LC_2H_2** ligand in $CDCl_3$.

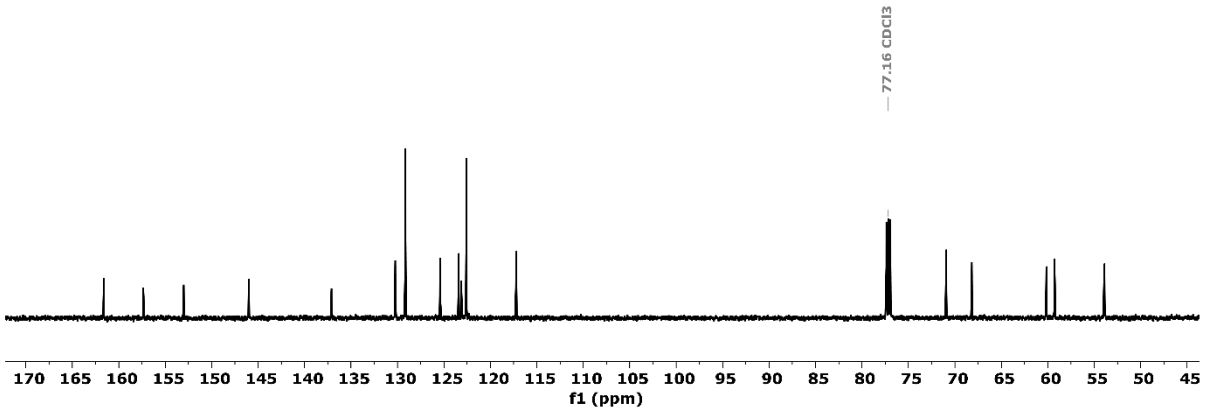

Fig. S14. ^{13}C NMR (151 MHz) spectrum of **LC_2H_2** ligand in $CDCl_3$.

2.1.4. Mass spectrometry of macrocyclic ligands (Figures S15-S17)

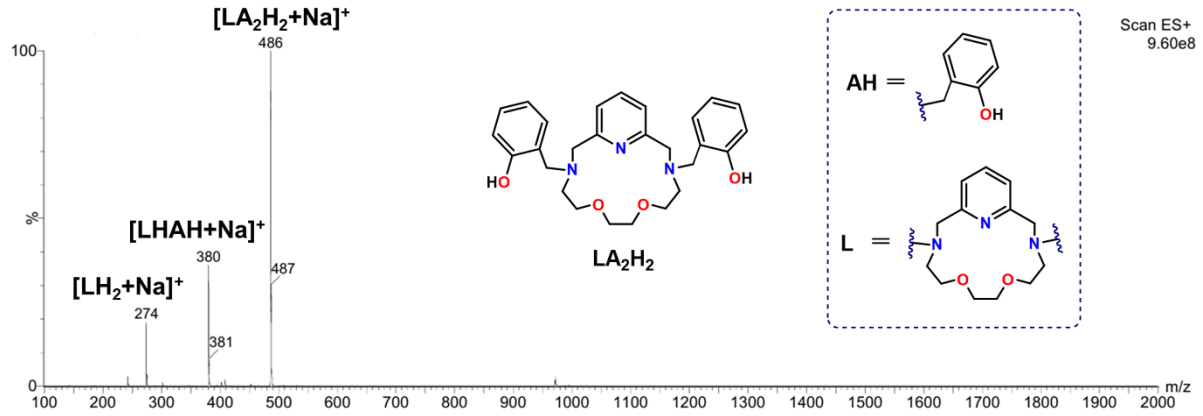

Fig. S15. ESI-MS spectra of the **LA_2H_2** ligand.

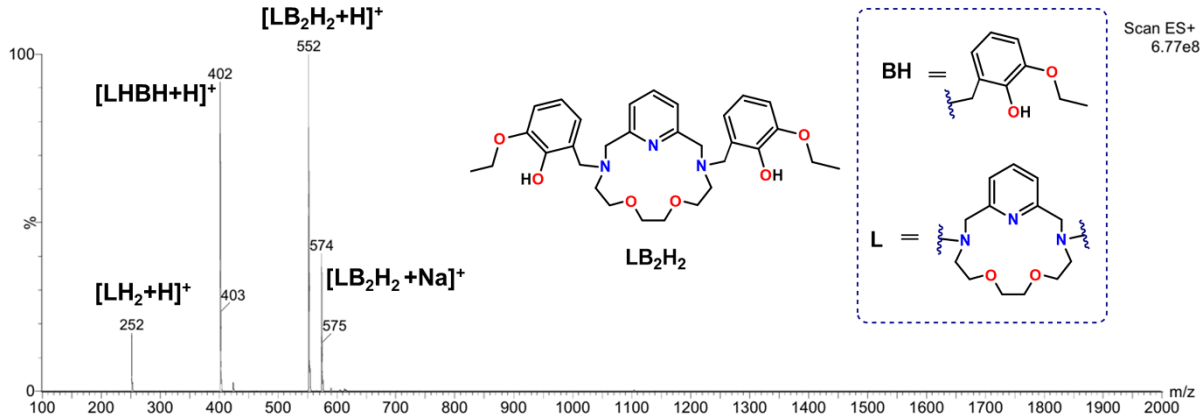

Fig. S16. ESI-MS spectra of the **LB_2H_2** ligand.

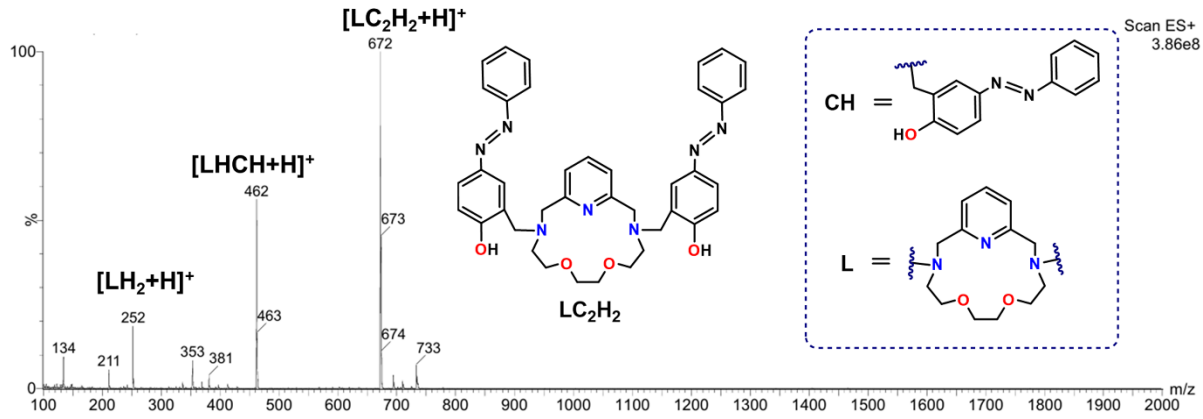

Fig. S17. ESI-MS spectra of the **LC_2H_2** ligand.

2.1.5. FT-IR spectroscopy of macrocyclic ligands and its complexes (Figures S18-S20)

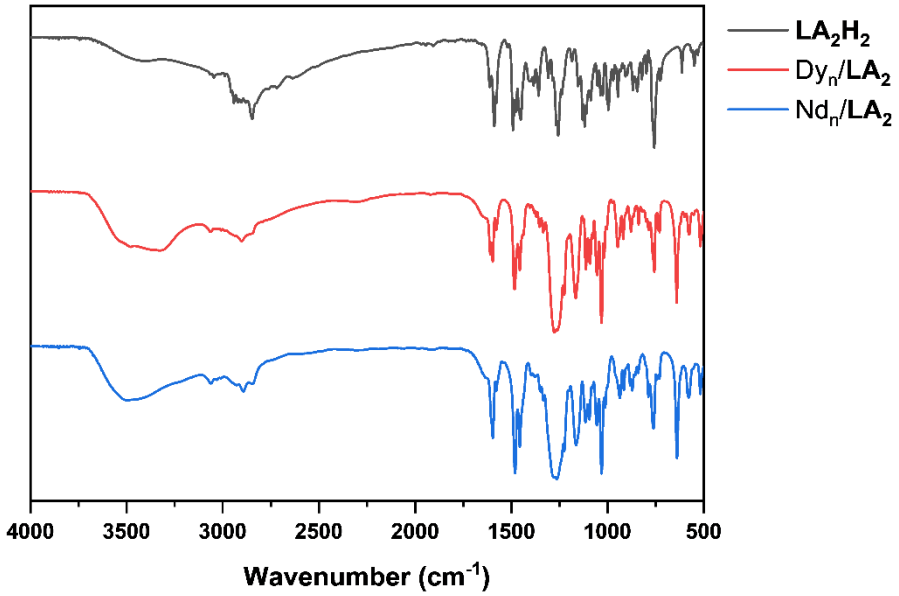

Fig. S18. FT-IR spectra of the **LA_2H_2** ligand and its macrocyclic lanthanide complexes.

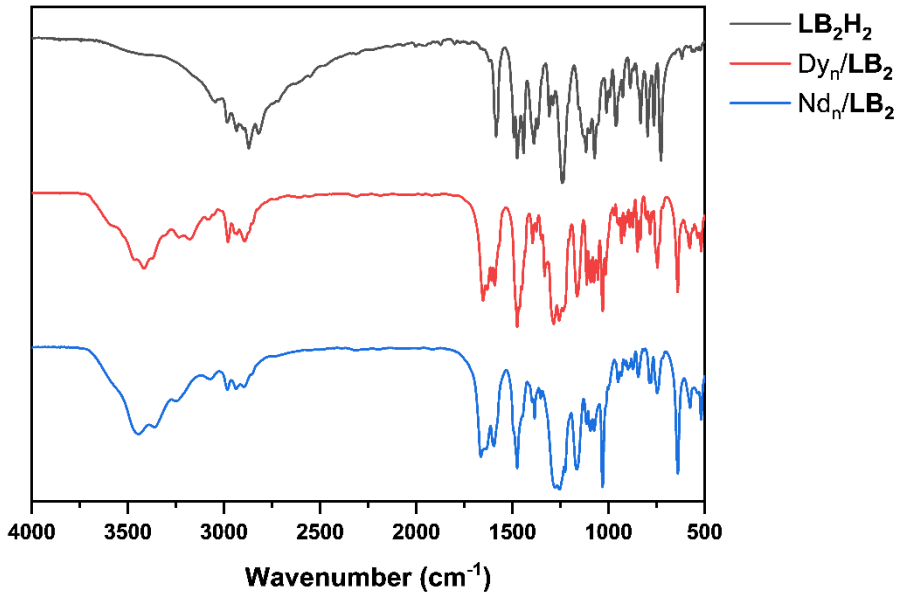

Fig. S19. FT-IR spectra of the **LB_2H_2** ligand and its macrocyclic lanthanide complexes.

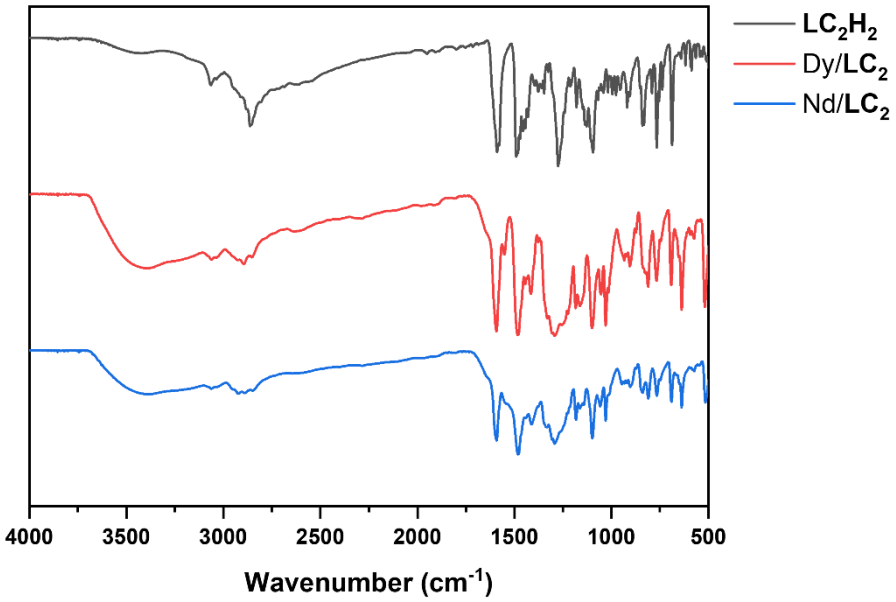

Fig. S20. FT-IR spectra of the LC_2H_2 ligand and its macrocyclic lanthanide complexes.

2.1.6. Mass spectrometry of macrocyclic lanthanide complexes (Figures S21-S28)

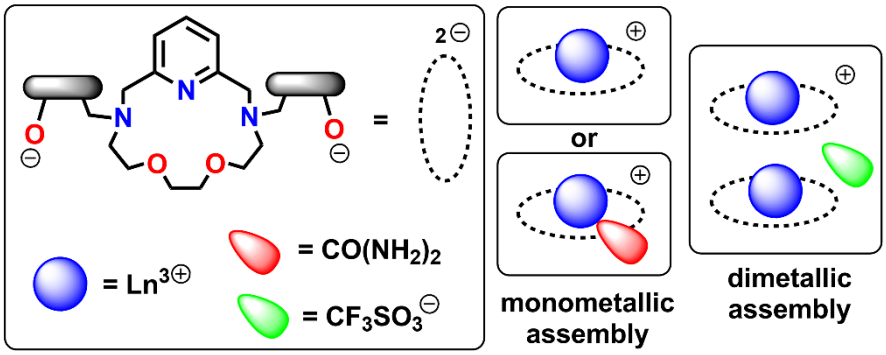

Fig. S21. Schematic representation of coordination motifs appearing on mass spectra of macrocyclic lanthanide complexes.

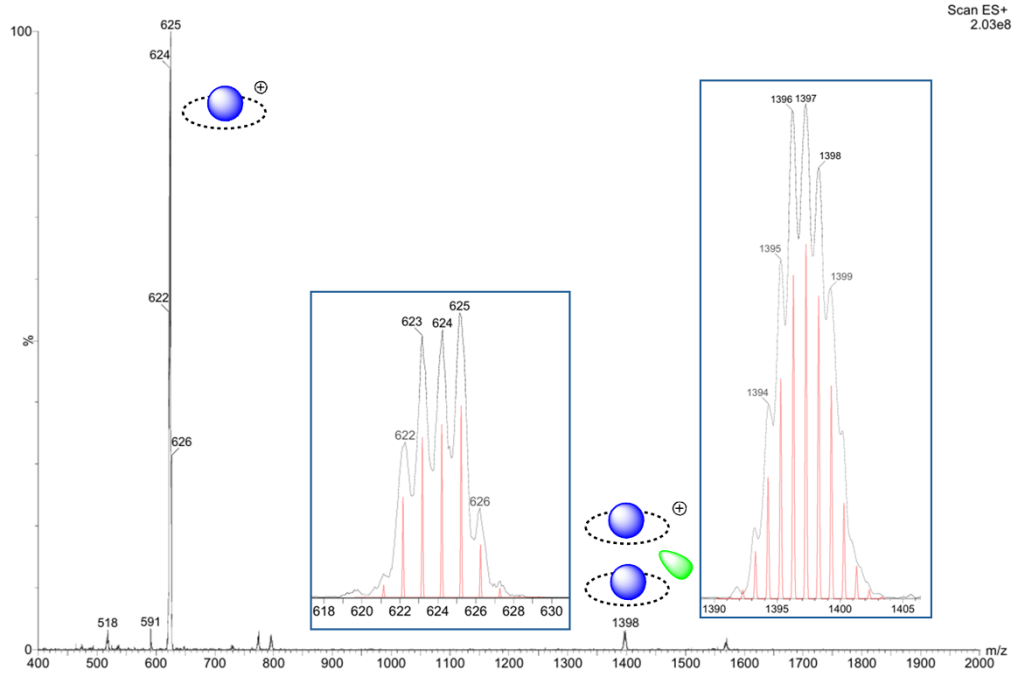

Fig. S22. ESI-MS spectra of the Dy/**LA_2** lanthanide complex. The insert graph (blue frame) presents comparison of experimental isotopic (grey) distribution with theoretical distribution (red) of Dy^{3+} ions.

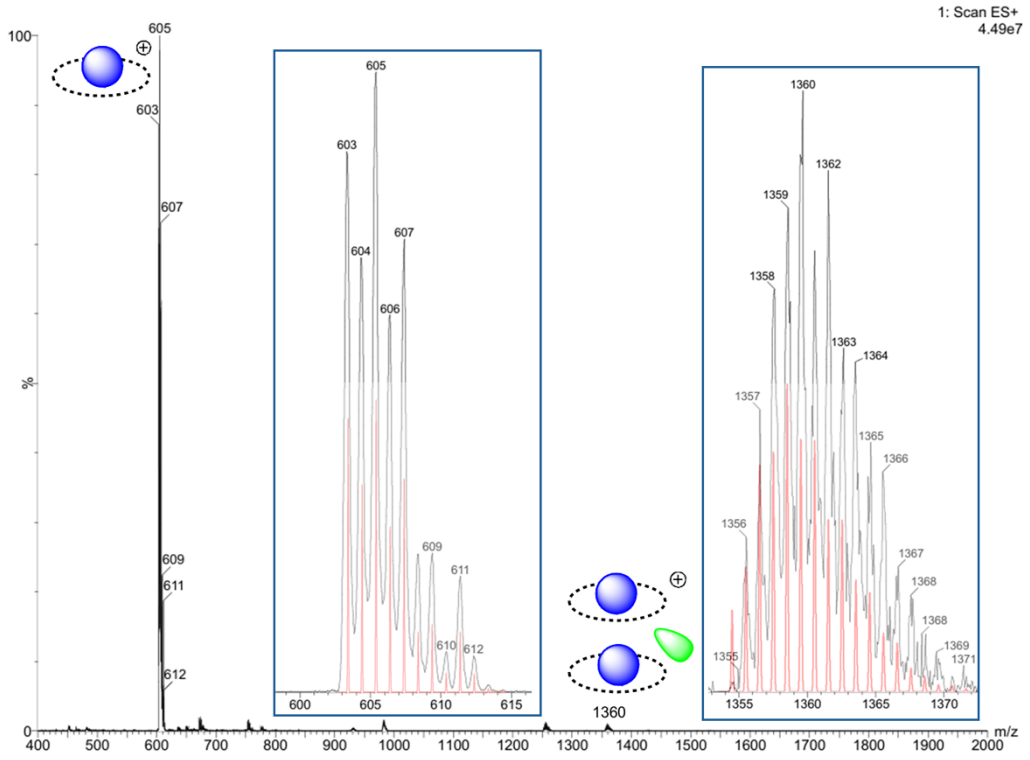

Fig. S23. ESI-MS spectra of the Nd/**LA_2** lanthanide complex. The insert graph (blue frame) presents comparison of experimental isotopic (grey) distribution with theoretical distribution (red) of Nd^{3+} ions.

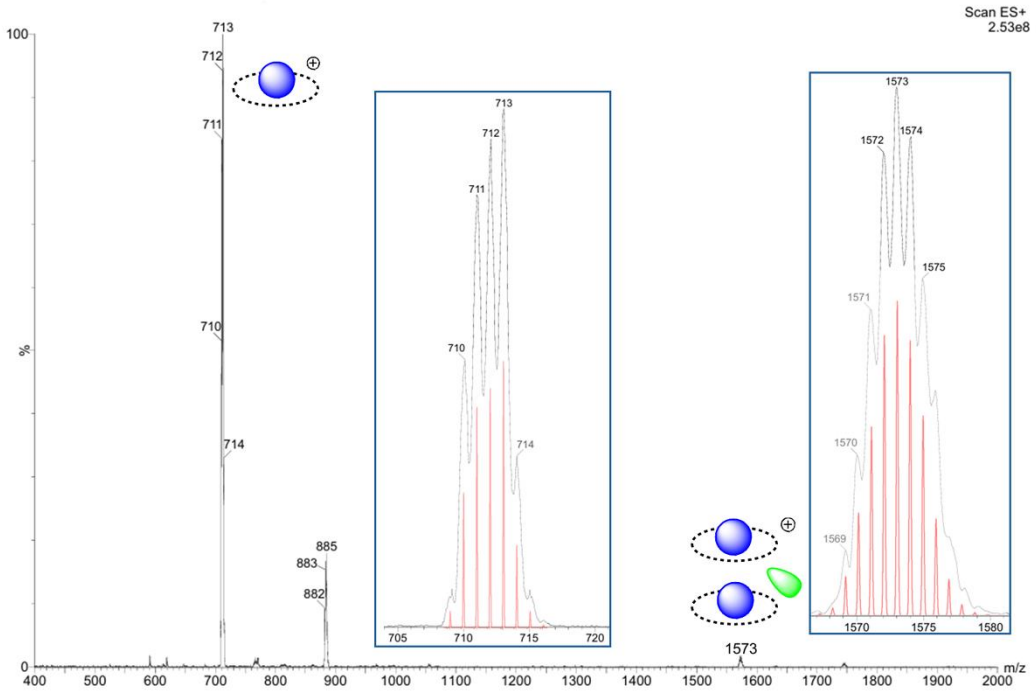

Fig. S24. ESI-MS spectra of the Dy/**LB_2**(DMSO) lanthanide complex. The insert graph (blue frame) presents comparison of experimental isotopic (grey) distribution with theoretical distribution (red) of Dy^{3+} ions.

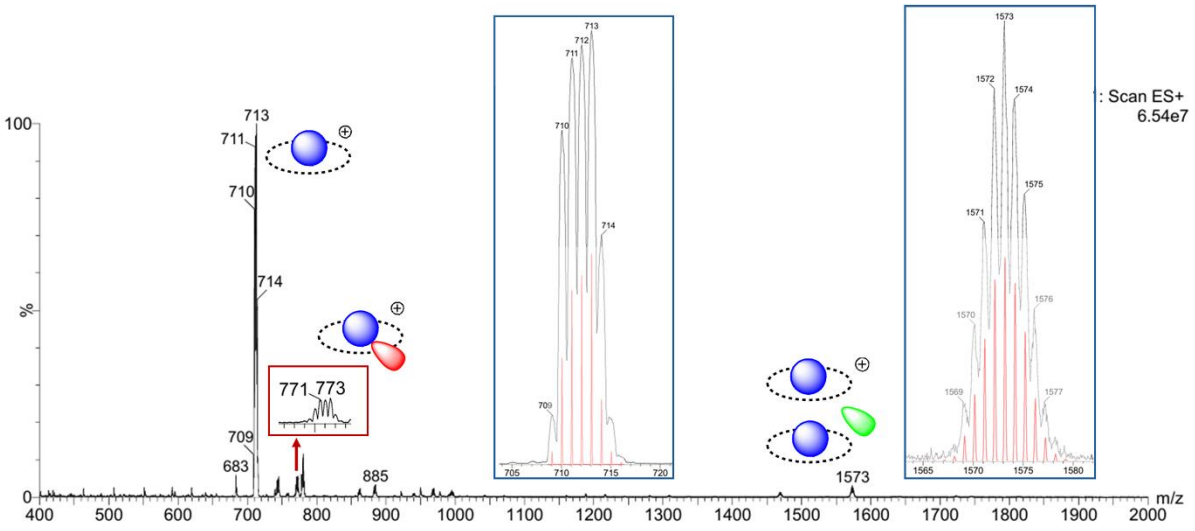

Fig. S25. ESI-MS spectra of the Dy/**LB_2** lanthanide complex. The insert graph (blue frame) presents comparison of experimental isotopic (grey) distribution with theoretical distribution (red) of Dy^{3+} ions.

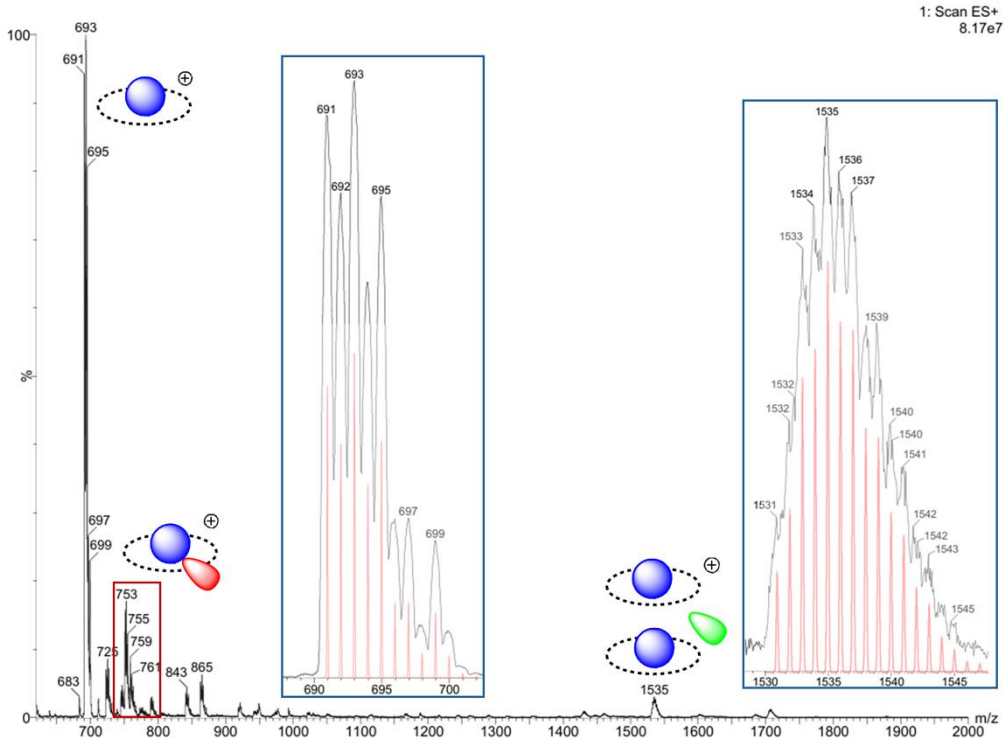

Fig. S26. ESI-MS spectra of the Nd/**LB_2** lanthanide complex. The insert graph (blue frame) presents comparison of experimental isotopic (grey) distribution with theoretical distribution (red) of Nd^{3+} ions.

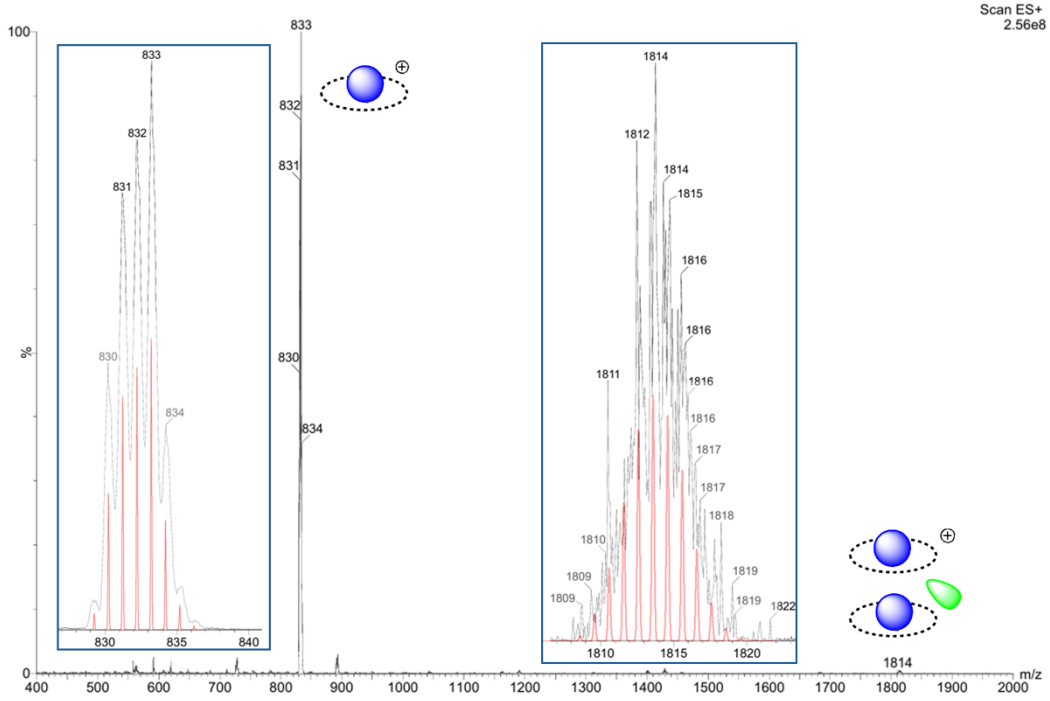

Fig. S27. ESI-MS spectra of the Dy/**LC_2** lanthanide complex. The insert graph (blue frame) presents comparison of experimental isotopic (grey) distribution with theoretical distribution (red) of Dy^{3+} ions.

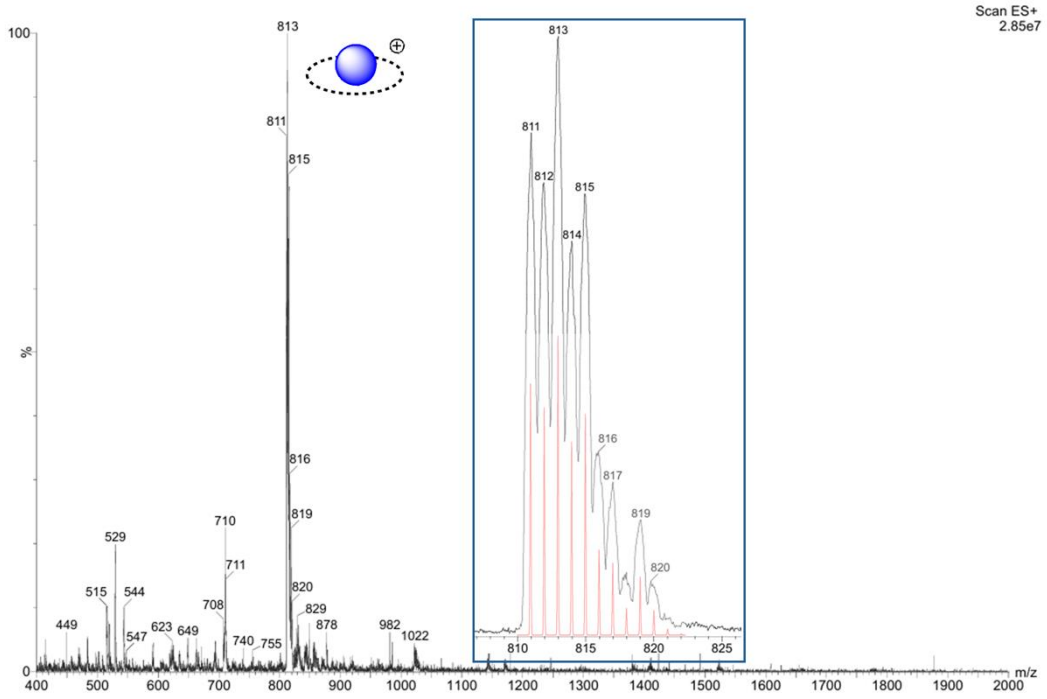

Fig. S28. ESI-MS spectra of the Nd/**LC_2** lanthanide complex. The insert graph (blue frame) presents comparison of experimental isotopic (grey) distribution with theoretical distribution (red) of Nd^{3+} ion.

3. X-ray crystallography (Tables S1-S5, Figure S29)

Diffraction data were collected by the ω-scan technique, for **1**, **3**, **5 - 9** and **11 - 14**: using graphite-monochromated MoK_α radiation (λ=0.71073 Å), at 100(1) K on Rigaku XCalibur four-circle diffractometer with EOS CCD detector, for **2** and **4** at 130(1) K, with mirror-monochromated CuK_α radiation (λ=1.54178 Å), at 130(1) on Rigaku SuperNova four-circle diffractometer with Atlas CCD detector, and for **10** at 100(1) K on a Bruker D8 QUEST KAPPA diffractometer with a microfocus sealed tube using a multilayer mirror as monochromator (CuK_α radiation, λ=1.54178 Å)and a Bruker PHOTON III CPAD detector. The data were corrected for Lorentz-polarization as well as for absorption effects. The structures were solved with SHELXT[6] and refined with the full-matrix least-squares procedure on F^2 by SHELXL.[7] All non-hydrogen atoms were refined anisotropically. Hydrogen atoms were placed in idealized positions and refined as 'riding model' with isotropic displacement parameters set at 1.2 times U_{eq} of appropriate carrier atoms. In some cases (**7**, **10**, **11**, **12**, **14**) large areas of highly diffused electron density distribution were detected; as the attempts to model highly disordered solvent molecules failed, the SQUEEZE procedure[8] was used. The details are listed in Table S1-S5.

Crystallographic data for the structural analysis has been deposited with the Cambridge Crystallographic Data centers re. Copies of this information may be obtained free of charge from: The Director, CCDC, 12 Union Road, Cambridge, CB2 1EZ, UK; e-mail: deposit@ccdc.cam.ac.uk, or www: www.ccdc.cam.ac.uk.

Table S1. Crystal data, data collection and structure refinement.

Compound	**(1)** $\mathbf{LB_2H_2}$	**(2)** $\mathbf{LH_2^{2+}B_2H_2}$ $\cdot\mathbf{2HC_2O_4^-}$	**(3)** $\mathbf{LH_2^{2+}B_2H_2}$ $\cdot\mathbf{2CF_3SO_3^-}$	**(7)** Dy$\mathbf{LB_2}$(DMSO)	**(9)** Dy$\mathbf{LB_2}$(urea)	**(12)** Nd$\mathbf{LB_2}$(urea)
Formula	$C_{31}H_{41}N_3O_6$	$C_{31}H_{43}N_3O_6^{+}\cdot C_4O_8H^{-}$ $\cdot 2(CH_3OH)\cdot H_2O$	$C_{31}H_{43}N_3O_6^{2+}\cdot$ $2(CF_3SO_3)^{-}$	$C_{33}H_{44}DyN_3O_7S$ $\cdot H_2O$	$C_{32}H_{43}DyN_5O_7^{+}\cdot$ $CF_3SO_3^{-}\cdot C_2H_3N$	$C_{32}H_{43}N_5NdO_7$
Formula weight	551.67	812.83	851.82	808.29	962.34	753.95
Crystal system	monoclinic	monoclinic	monoclinic	orthorhombic	orthorhombic	orthorhombic
Space group	$P2_1/n$	$P2_1/n$	$P2_1/c$	$P2_12_12_1$	$P2_12_12_1$	$P2_12_12_1$
a(Å)	11.1802(5)	13.3260(2)	10.3365(4)	12.64591(15)	7.89324(12)	7.89860(14)
b(Å)	17.0514(8)	22.7026(3)	16.0479(5)	12.95032(15)	19.1328(3)	19.2643(3)
c(Å)	15.3449(7)	14.3717(2)	23.0068(10)	24.1569(3)	24.8929(4)	24.9705(4)
β(°)	99.543(4)	112.7497(17)	92.507(4)	90	90	90
V(Å^3)	2884.8(2)	4009.68(11)	3812.7(3)	3956.14(8)	3759.32(10)	3799.54(11)
Z	4	4	4	4	4	4
D_x(g cm^{-3})	1.270	1.346	1.484	1.357	1.700	1.318
F(000)	1184	1732	1776	1648	1948	1544
μ(mm^{-1})	0.088	0.903	0.234	1.988	2.124	1.413
Reflections:						
collected	17882	18881	15531	33590	10354	30408
unique (R_{int})	6127 (0.0323)	8289 (0.0276)	7375 (0.0262)	7881 (0.0269)	6347 (0.0163)	8236 (0.0234)
with I>2σ(I)	4739	7130	5653	7125	6248	8106
R(F) [I>2σ(I)]	0.0446	0.0832	0.0603	0.0350	0.0254	0.0281
$wR(F^2)$ [I>2σ(I)]	0.0973	0.2189	0.1366	0.0912	0.0646	0.0623
R(F) [all data]	0.0635	0.0913	0.0829	0.0395	0.0259	0.0286
$wR(F^2)$ [all data]	0.1075	0.2258	0.1484	0.0941	0.0649	0.0626
Goodness of fit	1.015	1.084	1.076	1.024	1.075	1.068
max/min Δρ (e·Å^{-3})	0.26/-0.21	1.35/-0.92	0.65/-0.53	1.89/-0.78	2.14/-0.70	0.70/-1.05
CCDC deposition number	2478022	2478023	2478024	2478028	2478030	2478033

Table S2. Crystal data, data collection and structure refinement.

Compound	**(4)** $\mathbf{LH_2^{2+}C_2H_2}$ $\cdot\mathbf{2CF_3SO_3^-}$	**(5)** $\mathbf{LH_2^{2+}C_2H_2}$ $\cdot\mathbf{2CF_3SO_3^-}$	**(10)** Dy$\mathbf{LC_2}$(H_2O)	**(11)** $Dy_2(\mathbf{LC_2})_2(OH^-)$	**(14)** $Nd_2(\mathbf{LC_2})_2(OH^-)$
Formula	$C_{39}H_{43}N_7O_4^{2+}\cdot$ $2Cl^-\cdot 2(CH_3OH)$	$C_{39}H_{43}N_7O_4^{2+}\cdot$ $2(CF_3SO_3)^-\cdot C_2H_3N$	$C_{39}H_{40}DyN_7O_5\cdot$ $1/2(C_6H_6O_2)\cdot C_6H_{14}O$	$C_{78}H_{75}Dy_2N_{14}O_9^{+}\cdot$ $CF_3SO_3^-$	$C_{78}H_{78}N_{14}Nd_2O_9^{+}\cdot$ $CF_3SO_3^-\cdot 1/3(C_2H_3N)$
Formula weight	808.78	1013.00	1006.51	1826.59	1806.78
Crystal system	monoclinic	triclinic	triclinic	trigonal	trigonal
Space group	$P2_1/c$	P-1	P-1	R-3	R-3
a(Å)	17.2048(5)	13.9854(3)	13.2872(3)	29.6295(5)	29.5276(5)
b(Å)	9.1940(2)	24.5585(5)	13.6807(3)	29.6295(5)	29.5276(5)
c(Å)	26.9494(6)	11.9217(2)	15.0500(3)	47.2607(8)	48.5240(6)
α (°)	90	79.401(3)	106.2890(10)	90	90
β(°)	92.604(2)	77.262(3)	96.4140(10)	90	90
γ (°)	90	65.392(4)	95.8350(10)	120	120
V(Å^3)	4258.48(18)	2345.63(18)	2584.02(10)	35931.8(14)	36639.0(13)
Z	4	2	2	18	18
D_x(g cm^{-3})	1.262	1.434	1.294	1.519	1.474
F(000)	1712	1052	1032	16524	16494
μ(mm^{-1})	1.807	0.203	8.157	1.959	1.362
Reflections:					
collected	18817	18273	50066	86750	73800
unique (R_{int})	7650 (0.0405)	9382 (0.0212)	9447 (0.0609)	14061 (0.0719)	14297 (0.0728)
with I>2σ(I)	5836	7552	8398	9447	10135
R(F) [I>2σ(I)]	0.0585	0.0445	0.0451	0.0740	0.0818
$wR(F^2)$ [I>2σ(I)]	0.1612	0.1082	0.1165	0.1859	0.1939
R(F) [all data]	0.0771	0.0596	0.0527	0.1125	0.1149
$wR(F^2)$ [all data]	0.1745	0.1183	0.1234	0.2005	0.2099
Goodness of fit	1.084	1.044	1.040	1.226	1.021
max/min Δρ (e·Å^{-3})	0.43/-0.44	0.49/-0.35	1.40/-1.69	3.65/-1.17	3.51/-0.90
CCDC deposition number	2478025	2478026	2478031	2478032	2478035

Table S3. Crystal data, data collection and structure refinement.

Compound	**(6)** Na**LA$_2$H** (CH_3OH)	**(8)** Dy**LA$_2$**(H_2O)	**(13)** Nd_2(**LA$_2$**)$_2$(H_2O)$_2$
Formula	$C_{28}H_{36}N_3NaO_5$ ·CH_3OH	$C_{27}H_{33}DyN_3O_5^{+}$· $CF_3SO_3^{-}$·CH_3OH·H_2O	$C_{54}H_{66}N_6Nd_2O_{10}^{2+}$· $2(CF_3SO_3)^{-}$·$2(CH_3OH)$·C_2H_3N
Formula weight	549.63	841.19	1691.94.34
Crystal system	monoclinic	monoclinic	triclinic
Space group	$P2_1/n$	$P2_1/c$	P-1
a(Å)	10.18466(11)	12.5367(2)	10.79965(19)
b(Å)	13.91599(14)	18.3452(3)	12.2649(3)
c(Å)	20.2962(2)	15.0692(3)	13.4468(2)
α(°)	90	90	81.7313(16)
β(°)	101.4488(10)	111.423(2)	78.8461(15)
γ(°)	90	90	79.2425(16)
V(Å^3)	2819.34(5)	3226.29(11)	1706.01(6)
Z	4	4	1
D_x(g cm^{-3})	1.295	1.732	1.647
F(000)	1176	1692	858
μ(mm^{-1})	0.103	2.458	1.658
Reflections:			
collected	29214	14116	31954
unique (R_{int})	6473 (0.0180)	6486 (0.0244)	7722 (0.0275)
with I>2σ(I)	5698	5727	7233
R(F) [I>2σ(I)]	0.0381	0.0244	0.0223
wR(F^2) [I>2σ(I)]	0.0897	0.0532	0.0512
R(F) [all data]	0.0448	0.0300	0.0252
wR(F^2) [all data]	0.0943	0.0558	0.0523
Goodness of fit	1.022	1.071	1.062
max/min Δρ (e·Å^{-3})	0.46/-0.46	1.08/-0.69	1.05/-0.37
CCDC deposition number	2478027	2478029	2478034

Table S4 (A-C). Relevant geometric parameters describing the coordination of the ligand molecules.

A)

	(1)	**(2)**	**(3)**	**(7)**	**(9)**	**(12)**
N1C6C7N8	-59.79(18)	-68.6(3)	29.8(4)	-39.6(9)	-37.3(7)	40.5(6)
C6C7N8C9	153.24(13)	162.4(2)	-152.3(3)	164.4(7)	-71.1(6)	69.1(5)
C7N8C9C10	-73.96(16)	-79.6(3)	77.3(3)	-68.1(9)	92.7(5)	-90.3(5)
N8C9C10O11	-78.71(16)	-47.7(3)	47.7(4)	-40.5(11)	46.5(6)	-49.1(5)
C9C10O11C12	153.34(13)	-176.8(2)	77.2(4)	166.8(9)	152.0(5)	-156.1(4)
C10O11C12C13	-94.96(16)	-161.9(2)	-170.5(3)	-175.8(9)	-169.1(5)	172.6(4)
O11C12C13O14	179.38(12)	80.8(3)	63.0(3)	48.4(11)	-56.0(6)	56.8(6)
C12C13O14C15	168.79(13)	-172.4(2)	-178.9(3)	162.7(8)	-84.5(6)	86.6(6)
C13O14C15C16	95.68(16)	-173.9(2)	76.5(3)	176.2(7)	164.7(5)	-165.5(5)
O14C15C16N17	-64.50(19)	-52.3(3)	47.4(3)	-50.1(9)	-52.1(7)	55.3(7)
C15C16N17C18	-66.68(17)	-76.4(3)	76.8(3)	155.1(7)	-73.3(6)	70.6(6)
C16N17C18C2	164.23(12)	152.5(3)	-151.7(3)	-75.4(7)	163.5(5)	-160.5(5)
N17C18C2N1	-62.40(17)	-42.0(4)	44.6(4)	-29.8(9)	-32.7(7)	31.2(6)
C18C2N1C6	176.69(13)	178.8(2)	176.0(3)	-169.5(6)	178.3(5)	-179.6(4)
C2N1C6C7	-176.14(13)	-178.7(2)	176.1(3)	1176.5(7)	-173.7(5)	173.0(5)
C15C16N17C19	170.82(13)	157.9(3)	-157.0(3)	-86.2(9)	166.3(5)	-167.7(5)
C2C18N17C19	-72.77(15)	-83.7(3)	82.3(3)	162.4(6)	-79.0(5)	80.6(5)
C16N17C19C20	-76.52(16)	-174.4(2)	74.0(3)	53.0(9)	179.7(5)	-179.5(5)
C18N17C19C20	158.50(13)	60.2(3)	-159.2(3)	171.7(7)	60.5(6)	-58.2(6)
N17C19C20C29	148.30(14)	-113.7(3)	-96.2(3)	-119.0(8)	-114.6(6)	112.3(5)
N17C19C20C21	-37.44(20)	65.7(3)	79.3(3)	61.7(10)	69.7(7)	-70.1(7)
C6C7N8C30	-84.64(15)	-72.2(3)	82.5(3)	-76.7(8)	168.2(4)	-167.9(4)
C10C9N8C30	165.53(13)	155.3(2)	-157.0(3)	171.7(8)	-148.0(5)	149.0(4)
C7N8C30C31	158.12(13)	167.6(2)	-158.1(3)	64.9(9)	174.9(5)	-173.7(4)
C9N8C30C31	-80.04(16)	-66.4(3)	76.0(3)	-174.9(7)	53.4(6)	-50.6(5)
N8C30C31C32	-44.91(21)	-68.4(3)	87.3(3)	61.3(10)	58.8(7)	-61.3(6)
N8C30C31C40	141.54(16)	112.7(3)	-95.0(3)	121.8(8)	-119.2(6)	117.7(5)
A/B	87.62(5)	20.50(16)	34.83(10)	28.8(3)	29.1(2)	31.5(2)
A/C	45.12(4)	51.19(10)	54.22(10)	29.5(2)	33.1(2)	32.82(19)
B/C	75.52 (5)	68.33(8)	28.30(15)	28.0(3)	39.4(2)	40.51(18)
N1···N8	2.9036(18)	2.972(3)	2.703(4)	2.760(9)	2.765(6)	2.811(5)
N1···O11	4.3269(17)	3.894(3)	3.669(4)	3.854(9)	3.009(6)	3.092(5)
N1···O14	4.3413(18)	3.732(3)	3.569(4)	3.384(8)	4.062(6)	4.090(6)
N1···N17	2.8809(18)	2.804(3)	2.769(4)	2.756(9)	2.725(6)	2.766(6)
N8···O11	3.0736(17)	2.663(3)	2.765(4)	2.728(9)	2.725(6)	2.764(5)
N8···O14	5.3960(17)	4.736(3)	3.689(3)	4.221(9)	4.603(6)	4.693(5)
N8···N17	5.4043(18)	5.346(3)	4.681(4)	4.701(9)	4.696(7)	4.793(6)
O11···O14	3.5975(16)	2.991(3)	2.717(3)	2.596(8)	2.668(5)	2.711(5)
O11···N17	5.3331(17)	4.895(3)	3.924(4)	4.555(8)	3.834(6)	3,950(5)
O14···N17	3.0709(18)	2.728(3)	2.780(4)	2.803(8)	2.789(6)	2.816(6)

B)

	(6)	**(8)**	**(13)**
N1C6C7N8	-40.98(16)	-31.3(4)	-30.9(3)
C6C7N8C9	167.64(10)	159.5(2)	153.64(18)
C7N8C9C10	-67.51(13)	-70.4(3)	-57.8(2)
N8C9C10O11	-53.12(14	-47.2(3)	-36.3(2)
C9C10O11C12	169.50(10)	177.7(2)	170.95(18)
C10O11C12C13	-162.42(10)	-171.8(2)	-135.53(19)
O11C12C13O14	58.70(13)	48.2(3)	-52.1(2)
C12C13O14C15	176.02(10)	156.8(2)	-173.75(18)
C13O14C15C16	172.49(10)	174.1(2)	175.17(17)
O14C15C16N17	-77.46(13)	-51.0(3)	60.1(2)
C15C16N17C18	162.27(10)	157.4(2)	71.5(2)
C16N17C18C2	-72.56(13)	-73.6(3)	-84.6(2)
N17C18C2N1	-23.59(16)	-34.6(4)	-31.0(3)
C18C2N1C6	-173.75(11)	-169.8(2)	-169.50(19)
C2N1C6C7	-178.75(11)	177.9(3)	-179.07(19)
C15C16N17C19	-169.9(2)	-86.2(3)	-170.09(18)
C2C18N17C19	167.43(10)	166.1(2)	159.70(18)
C16N17C19C20	-168.32(10)	59.0(3)	-176.51(17)
C18N17C19C20	-48.23(14)	176.4(2)	-57.3(2)
N17C19C20C26	101.52(13)	-122.5(3)	102.9(2)
N17C19C20C21	-80.35(15)	59.8(4)	-74.4(2)
C6C7N8C27	-70.74(13)	-82.8(3)	-89.0(2)
C10C9N8C27	172.13(10)	169.9(2)	-177.91(17)
C7N8C27C28	173.15(10)	61.1(3)	57.3(2)
C9N8C27C28	-64.59(13)	-179.8(2)	178.14(17)
N8C27C28C29	-73.39(15)	67.5(3)	62.9(3)
N8C27C28C34	109.95(13)	-113.5(3)	-118.5(2)
A/B	83.03(4)		85.28(7)
A/C	59.25(5)		67.62(8)
B/C	48.89(3)		35.15(7)
N1···N8	2.8285(14)	2.764(3)	2.856(2)
N1···O11	4.1682(14)	3.874(3)	3.552(2)
N1···O14	3.5618(13)	3.468(3)	3.068(2)
N1···N17	2.7830(14)	2.788(3)	2.873(2)
N8···O11	2.8026(14)	2.744(3)	2.648(2)
N8···O14	4.2370(13)	2.744(3)	4.279(2)
N8···N17	4.8114(14)	4.751(3)	4.936(2)
O11···O14	2.7186(13)	2.586(3)	2.619(2)
O11···N17	4.8817(14)	4.571(3)	4.647(2)
O14···N17	3.0573(13)	2.780(3)	2.860(2)

C)

	(4)	**(5)**	**(10)**	**(11A)**	**(11B)**	**(14A)**	**(14B)**
N1C6C7N8	36.0(3)	59.2(2)	-33.8(6)	-32.3(15)	-39.9(11)	31.8(16)	23.6(13)
C6C7N8C9	-148.4(2)	-158.83(16)	161.0(4)	159.3(10)	162.3(8)	-157.3(11)	85.0(11)
C7N8C9C10	72.3(3)	81.9(2)	-69.3(5)	-62.2(13)	-61.2(10)	62.4(14)	-75.0(11)
N8C9C10O11	53.0(3)	51.6(2)	-42.9(5)	-44.5(14)	-38.9(10)	47.2(16)	-57.8(11)
C9C10O11C12	74.6(3)	172.64(17)	175.2(4)	165.18(11)	166.1(7)	-164.6(12)	-164.5(9)
C10O11C12C13	-169.2(2)	161.33(18)	-177.2(4)	-110.1(13)	-118.6(9)	106.9(12)	168.9(9)
O11C12C13O14	60.8(3)	-78.9(2)	51.0(6)	-56.4(13)	-52.1(12)	56.4(13)	53.3(10)
C12C13O14C15	-167.5(2)	173.67(18)	163.3(4)	-160.2(10)	-167.9(9)	162.6(10)	112.0(9)
C13O14C15C16	73.7(3)	176.83(17)	172.6(4)	165.1(9)	161.8(9)	-166.6(10)	-167.2(8)
O14C15C16N17	51.8(3)	49.5(2)	-53.5(5)	56.8(11)	60.1(12)	-53.7(13)	45.7(10)
C15C16N17C18	72.3(3)	76.0(2)	154.1(4)	70.7(11)	71.5(11)	-76.3(12)	60.8(10)
C16N17C18C2	-150.8(2)	-163.84(18)	-75.7(5)	-82.4(10)	-80.2(11)	81.6(11)	-160.2(8)
N17C18C2N1	38.8(3)	52.1(2)	-33.9(6)	-25.6(13)	-29.6(12)	28.2(14)	38.4(12)
C18C2N1C6	177.4(2)	178.17(17)	-168.0(4)	-173.7(9)	-170.3(8)	172.1(10)	180.0(8)
C2N1C6C7	178.6(2)	179.40(17)	178.7(4)	177.2(10)	-178.5(8)	-178.2(10)	172.7(8)
C15C16N17C19	-162.0(2)	-158.89(17)	-89.3(5)	-170.9(8)	-172.6(9)	166.6(10)	-57.7(8)
C2C18N17C19	85.8(3)	70.1(2)	163.2(4)	160.1(8)	164.1(9)	-162.3(9)	79.2(10)
C16N17C19C20	-166.6(2)	59.2(2)	55.9(5)	176.7(7)	173.1(9)	-177.3(9)	177.9(8)
C18N17C19C20	-41.2(3)	-175.05(15)	174.0(4)	-64.6(9)	-67.5(10)	64.3(10)	-59.2(10)
N17C19C20C34	99.0(3)	-115.1(2)	-124.8(4)	111.0(9)	104.8(11)	-107.5(10)	125.9(9)
N17C19C20C21	-81.2(3)	64.0(2)	58.1(6)	-72.1(10)	-70.0(12)	72.8(10)	-60.5(11)
C6C7N8C35	88.5(3)	74.91(19)	-80.7(5)	-83.2(12)	-78.1(10)	83.6(13)	-159.6(9)
C10C9N8C35	-162.0(2)	-152.80(17)	169.7(4)	177.8(9)	177.7(7)	-176.0(10)	168.4(9)
C7N8C35C36	-44.3(3)	-167.29(16)	59.2(5)	60.7(12)	62.6(10)	-57.4(12)	65.3(11)
C9N8C35C36	-169.6(2)	66.7(2)	179.1(3)	-177.2(9)	-177.7(7)	179.7(10)	-176.8(9)
N8C35C36C37	-76.0(3)	67.4(2)	69.4(5)	59.6(14)	58.1(11)	-64.5(14)	76.3(13)
N8C35C36C50	105.2(3)	-112.3(2)	-115.3(5)	-124.7(10)	-128.5(9)	119.1(11)	-103.1(13)
A/B	21.66(7)	50.39(6)	20.80(17)	83.5(3)	88.4(3)	83.2(3)	34.6(2)
A/C	36.51(6)	74.51(7)	33.33(16)	83.7(2)	71.8(3)	78.1(3)	72.5(3)
B/C	23.90(8)	58.28(7)	32.42(13	36.5(3)	35.1(2)	37.3(4)	87.1(3)
N1···N8	2.721(3)	2.853(2)	2.778(5)	2.789(13)	2.818(10)	2.803(15)	2.854(13)
N1···O11	3.640(3)	3.844(2)	3.833(5)	3.767(10)	3.716(9)	3.823(12)	3.045(10)
N1···O14	3.687(3)	3.857(2)	3.434(5)	2.888(10)	2.938(9)	2.952(11)	3.853(10)
N1···N17	2.732(3)	2.815(2)	2.796(5)	2.872(11)	2.847(12)	2.877(11)	2.876(11)
N8···O11	2.872(3)	2.711(2)	2.709(5)	2.691(12)	2.658(10)	2.720(13)	2.852(11)
N8···O14	3.810(3)	4.792(2)	4.262(5)	4.012(14)	4.081(10)	4.048(14)	4.737(11)
N8···N17	4.670(3)	5.207(2)	4.753(5)	4.862(12)	4.876(11)	4.892(12)	4.924(12)
O11···O14	2.713(3)	2.960(2)	2.603(5)	2.646(11)	2.641(9)	2.668(13)	2.670(10)
O11···N17	3.754(3)	4.712(2)	4.588(5)	4.693(10)	4.653(10)	4.734(12)	4.129(10)
O14···N17	2.870(3)	2.672(2)	2.830(5)	2.828(9)	2.803(11)	2.844(11)	2.720(10)

Table S5. The coordination of the metal centers. The inserted graphs illustrate labelled coordination atoms from representative complexes.

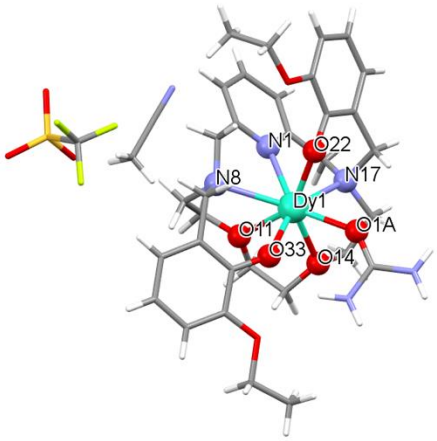

Compound 9

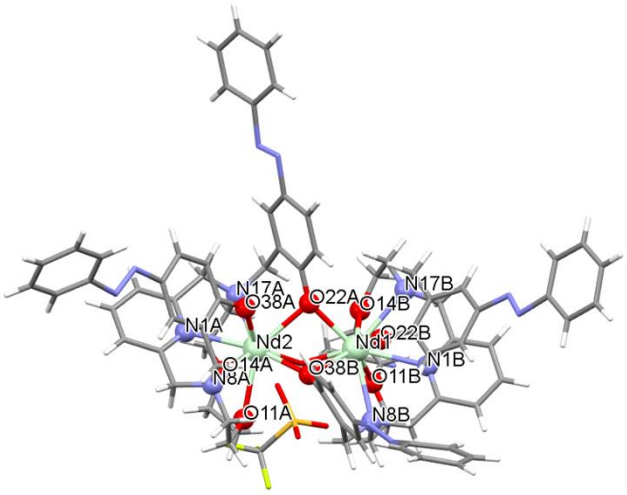

Compound 14

	(7)	(8)	(9)	(10)	(11A)	(11B)	(12)	(13)	(14A)	(14B)
Ln-N1	2.520(6)	2.512(2)	2.517(4)	2.507(3)	2.565(7)	2.580(7)	2.600(4)	2.5854(17)	2.677(7)	2.643(8)
Ln-N8	2.593(6)	2.597(2)	2.617(4)	2.598(3)	2.708(9)	2.749(7)	2.680(4)	2.7628(17)	2.711(8)	2.765(9)
Ln-O11	2.484(5)	2.4662(19)	2.488(4)	2.478(3)	2.579(7)	2.536(6)	2.573(3)	2.6559(15)	2.601(6)	2.612(7)
Ln-O14	2.530(5)	2.481(2)	2.495(4)	2.509(3)	2.558(7)	2.540(6)	2.567(3)	2.7196(15)	2.590(7)	2.599(8)
Ln-N17	2.581(6)	2.620(2)	2.567(5)	2.603(3)	2.647(7)	2.638(7)	2.663(4)	2.6723(17)	2.782(8)	2.686(8)
Ln-O22	2.176(5)	2.2059(19)	2.202(4)	2.189(3)	2.219(6)	2.226(6)	2.254(3)	2.2873(14)	2.314(6)	2.295(6)
Ln-O33	2.197(5)	2.2072(19)	2.204(4)	2.224(3)	2.253(5)	2.246(6)	2.271(3)	2.3754(14)	2.329(6)	2.344(6)
Ln-O1A	2.360(5)	2.359(2)	2.340(4)	2.364(3)	2.309(6)	2.302(5)	2.419(3)	2.5062(16)	2.405(6)	2.395(7)

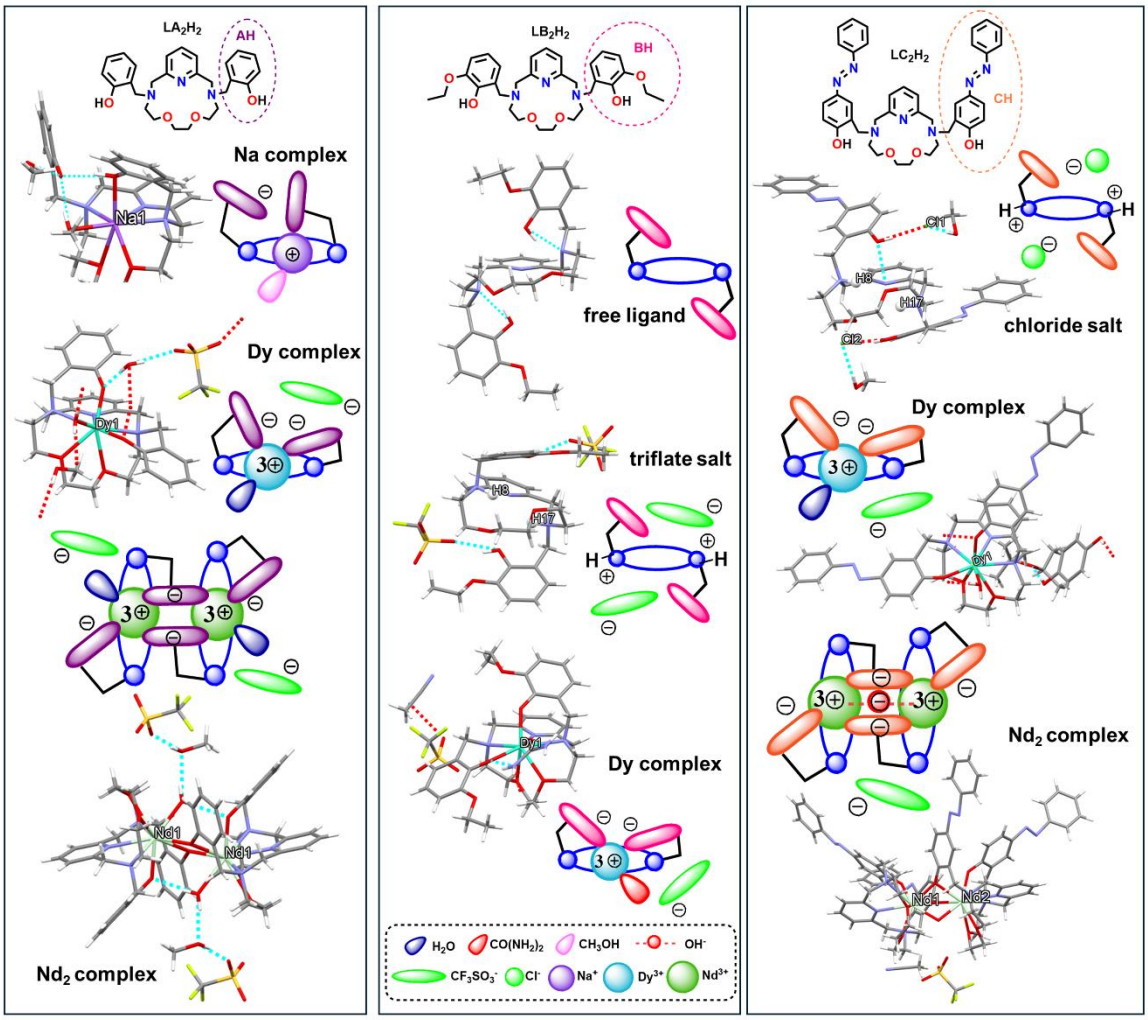

Fig. S29. Schematic representation of the conformations of free ligands, its sodium complex or protonated salts forms, and selected complexes with lanthanide ions (Ln^{3+}), based on X-ray crystallographic data. Inserted crystal X-ray structures include pointed hydrogen bonds, coordinating solvent molecules to the Ln^{3+} centre, counterions and solvent molecules in the outer coordination sphere. On graphical schemes, solvent molecules present in the crystal lattice of the complexes have been omitted, only the first coordination sphere around the Ln^{3+} ion is presented. In the complexes with lanthanide ions, all macrocyclic arms are deprotonated, whereas in the case of the free ligand and its protonated salts all are in the - OH form. In the sodium complex one arm remains deprotonated and the other is in the OH form.

4. NMR and mass spectroscopy of diamagnetic Ln^{3+}-assemblies (Figure S30)

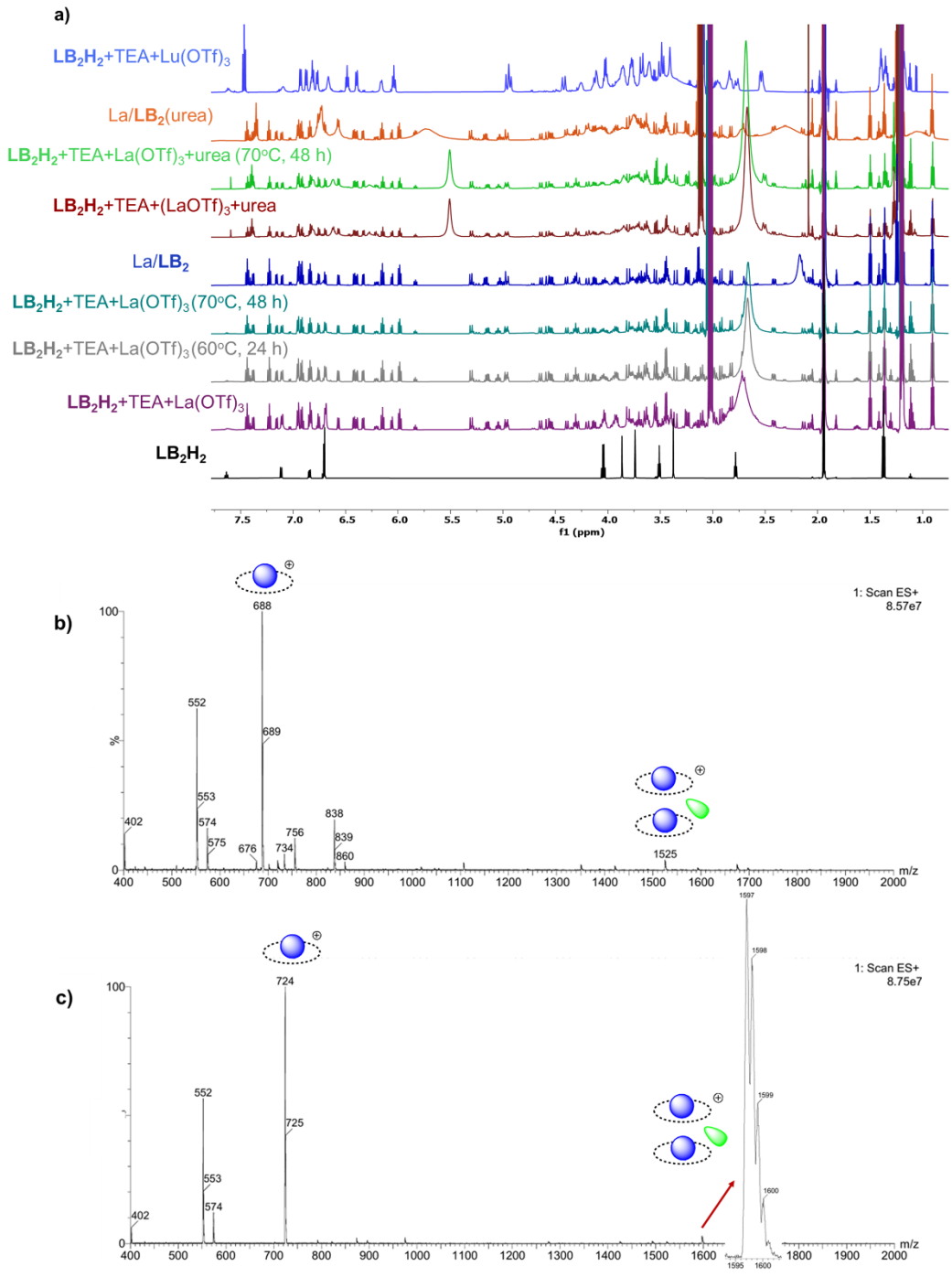

Fig. S30. ^{1}H NMR (CD_3CN) characterization of **LB_2H_2** macrocyclic ligand and its La^{3+} and Lu^{3+} assemblies (a) with illustrative examples showing their appearance in the mass spectra of the lanthanum(III) and lutetium(III) complexes obtained *in situ* (b and c).

5. Corelation of structural and optical properties: PXRD, luminescence and DFT studies (Figures S31-S35)

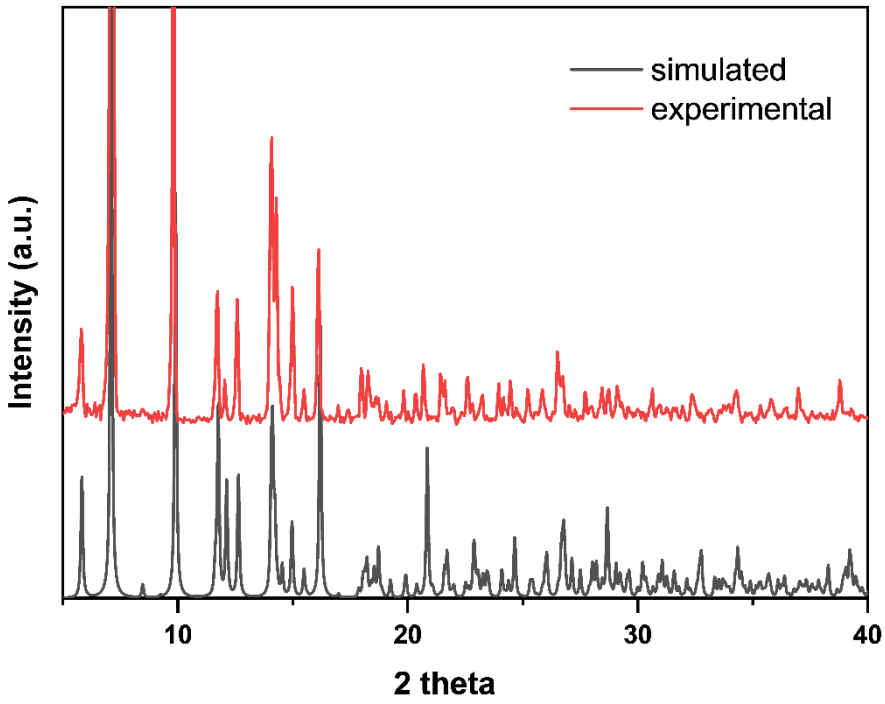

Fig. S31. Comparison of experimental PXRD pattern for investigated Dy/**LB_2** complex and simulated PXRD pattern for obtained monometallic Dy**LB_2**(urea) crystals.

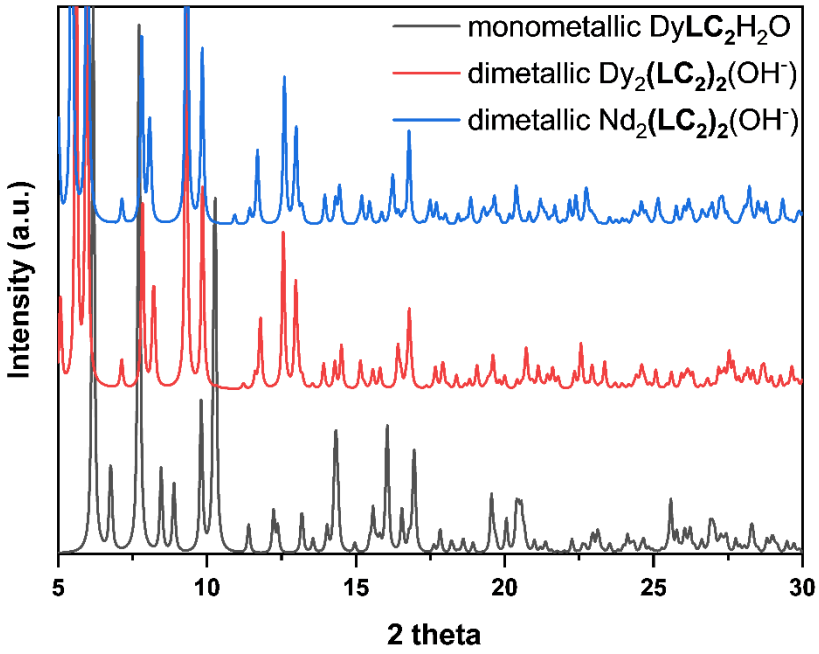

Fig. S32. Comparison of simulated PXRD patterns for mono- and dimetallic Ln^{3+} complexes based on **LC_2** moiety.

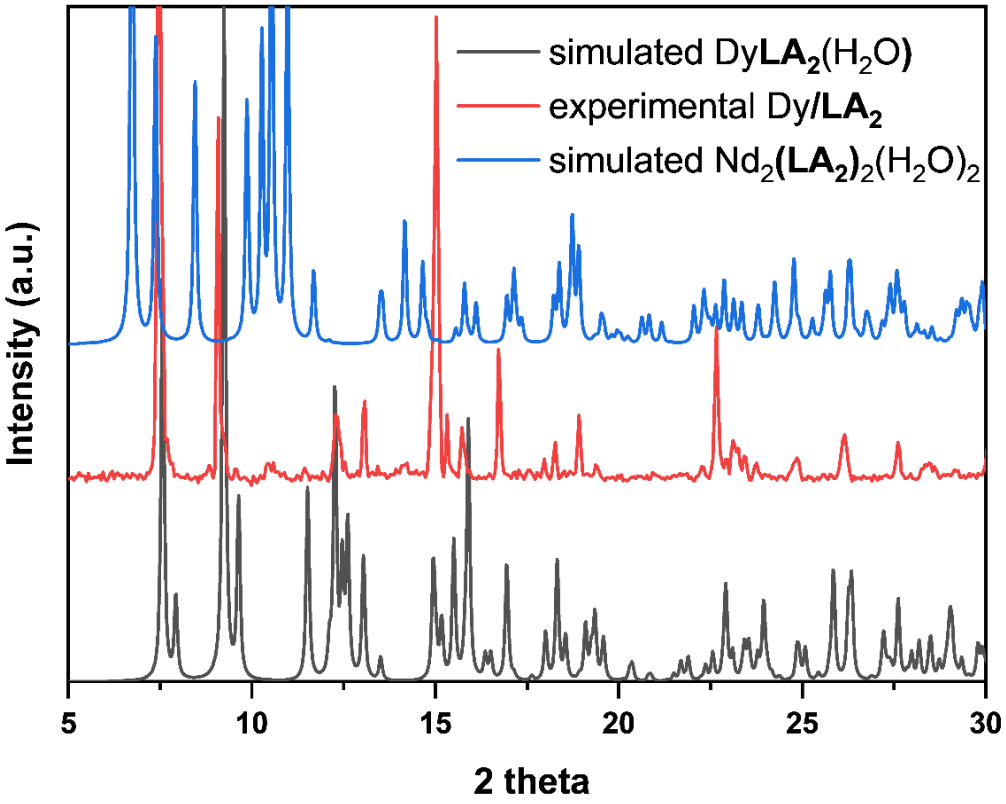

Fig. S33. Comparison of experimental PXRD pattern for investigated Dy/**LA**$_2$ complex and simulated PXRD pattern for obtained monometallic Dy**LA**$_2$(H_2O) crystals and dimetallic Nd_2(**LA**$_2$)$_2$(H_2O)$_2$ crystals.

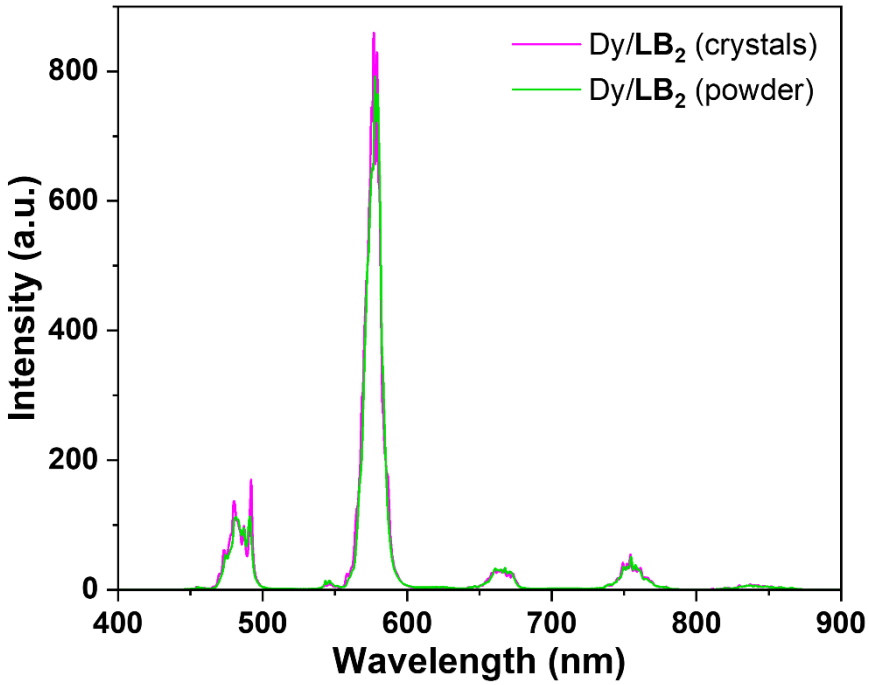

Fig. S34. Comparison of solid-state emission spectra of Dy/**LB**$_2$ systems in the form of crystals and powder. Dy/**LB**$_2$ (crystals) = Dy**LB**$_2$(urea) monocrystals resolved by X-ray, obtained by slow evaporation method; Dy/**LB**$_2$ (powder) = complex in the powder form, obtained by precipitation with diethyl ether.

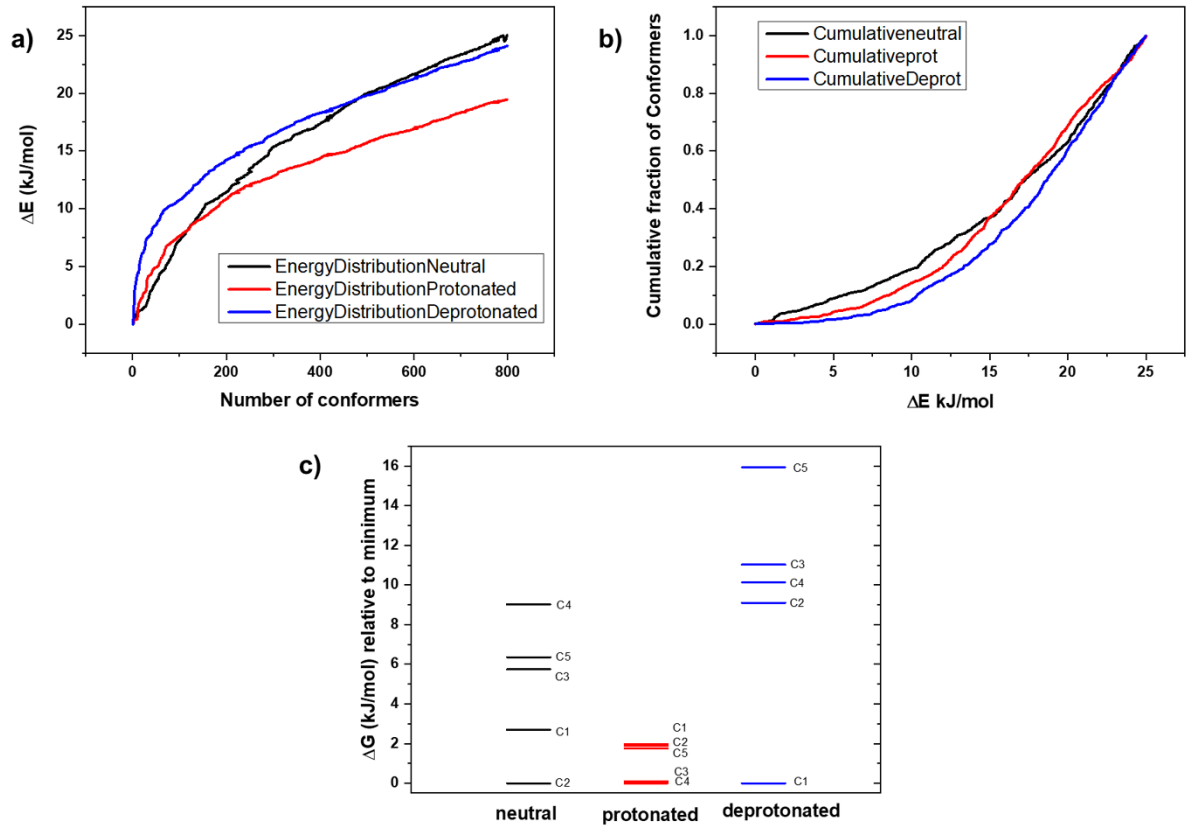

Fig. S35. Comparative Energy Distribution plot (a), the corresponding Cumulative Energy Distribution plot (b) and relative Gibbs free energies of representative low-energy conformers optimized at the DFT level (c).

6. Thermogravimetric analysis of macrocyclic lanthanide complexes (Figures S36-S37)

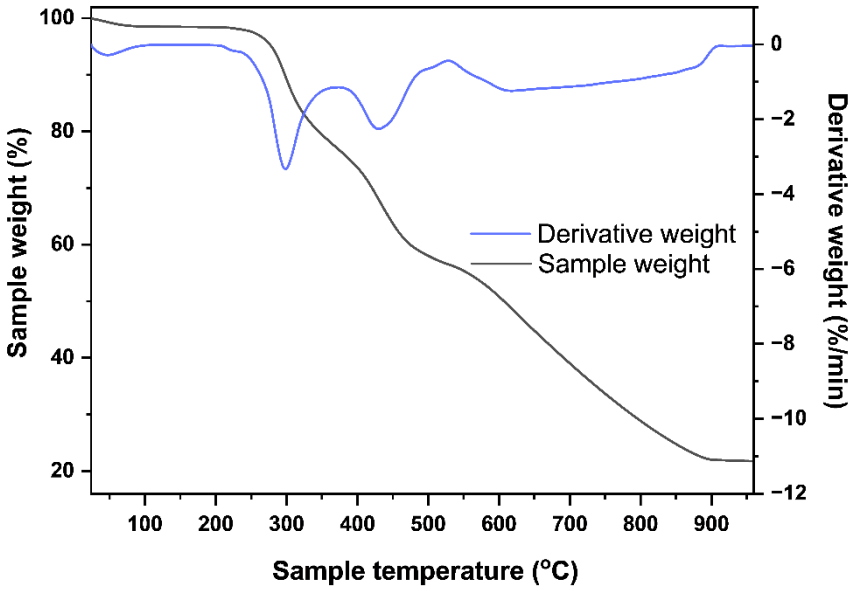

Fig. S36. TGA plot of Dy/**LB_2** lanthanide complex.

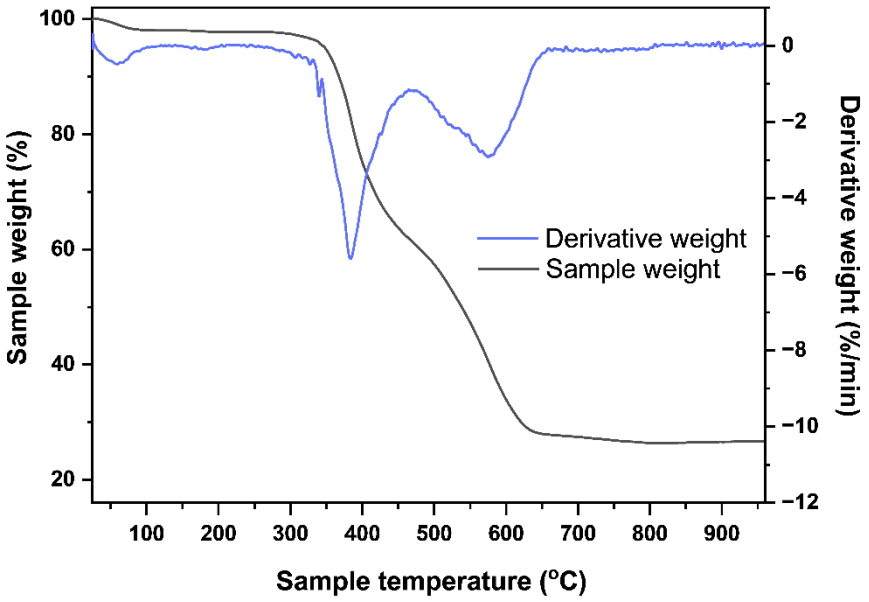

Fig. S37. TGA plot of Nd/**LA$_2$** lanthanide complex.

7. Luminescence studies (Figures S38-S40)

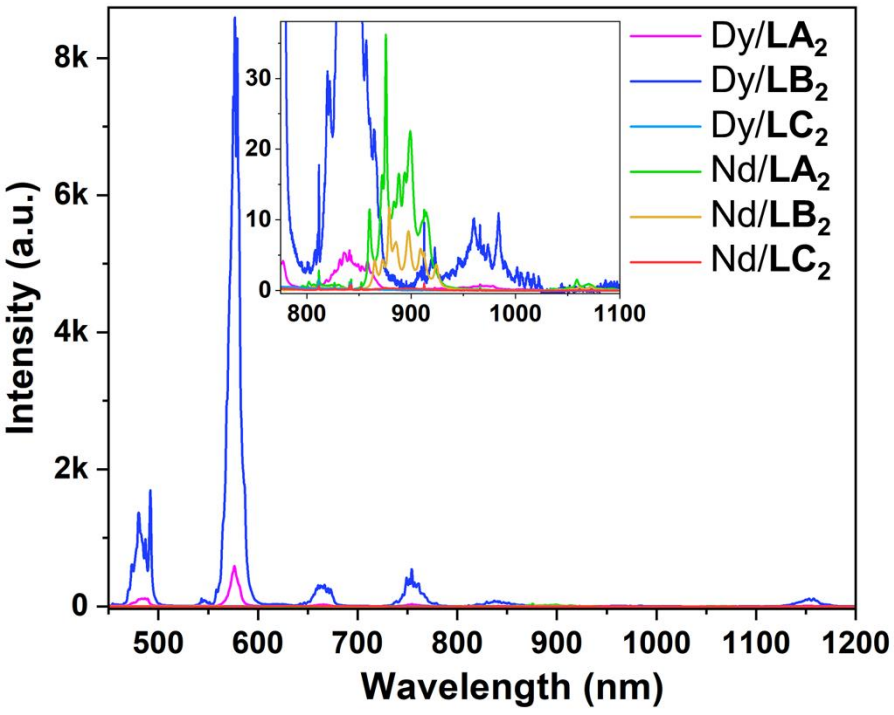

Fig. S38. Emission spectra of the different lanthanide macrocyclic complexes at ambient conditions recorded at 370 nm excitation.

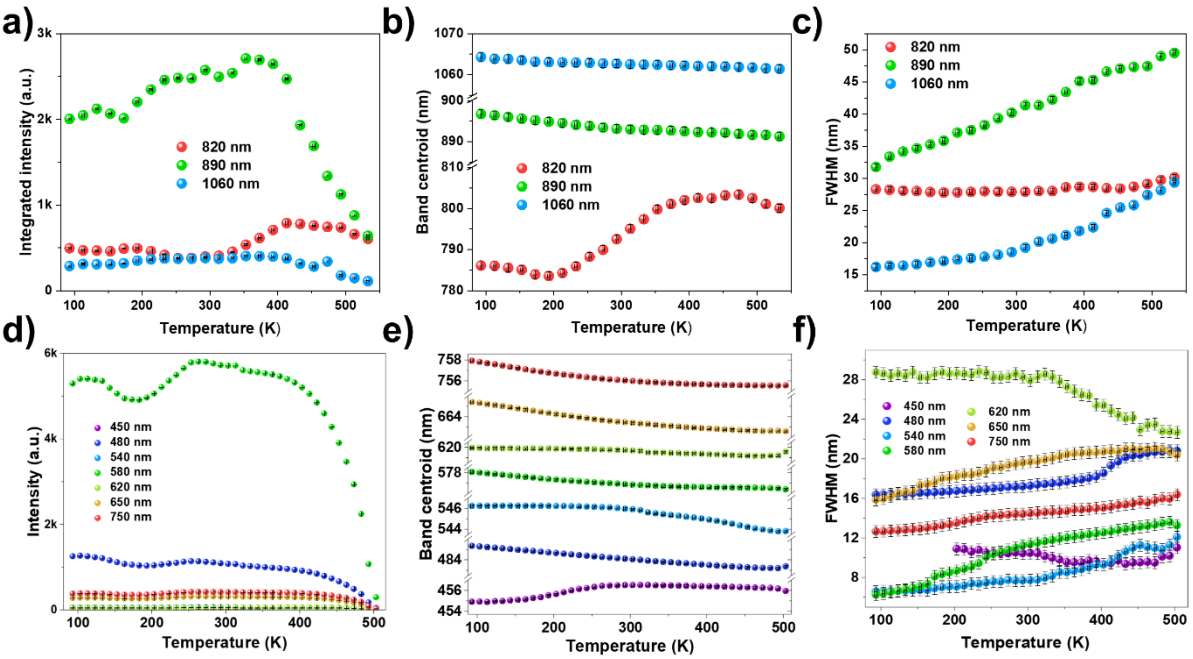

Fig. S39. Integrated emission intensity for the Nd/**LA$_2$** (a) and Dy/**LB$_2$** (d) macrocyclic complexes, calculated band centroids for the Nd^{3+} (b) and Dy^{3+} (e) complexes, and FWHM values of the Nd^{3+} (c) and Dy^{3+} (f) emission bands as a function of modified temperature.

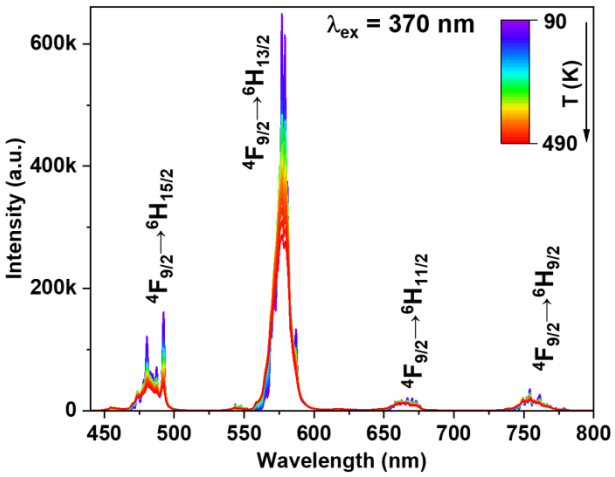

Fig. S40. Detailed emission spectra of the Dy/**LB$_2$** macrocyclic complex under varied temperature conditions recorded at 370 nm excitation.

8. Photoisomerization studies (Figures S41-S42)

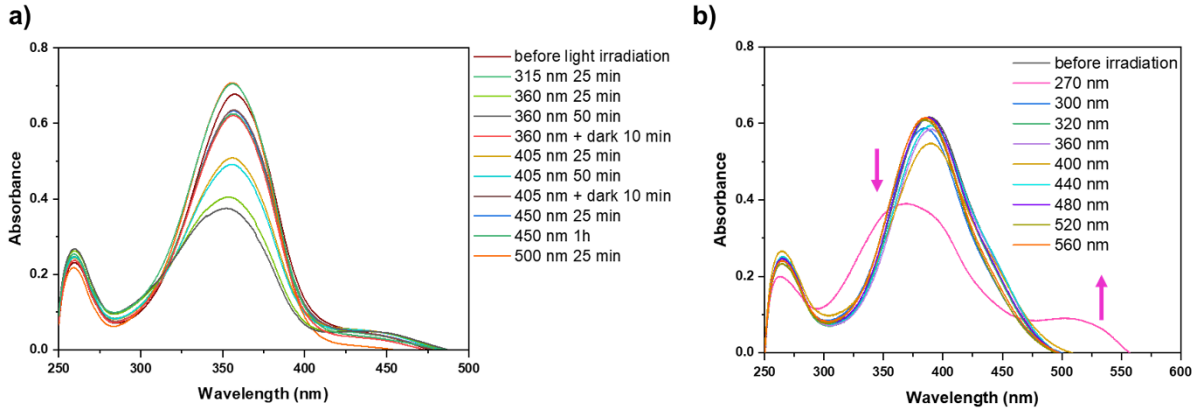

Fig. S41. UV-Vis absorption spectra before and after light irradiation (under specified conditions) for **LC_2H_2** ligand (a) and Nd/**LC_2** lanthanide complex (time of irradiation 30 min) (b).

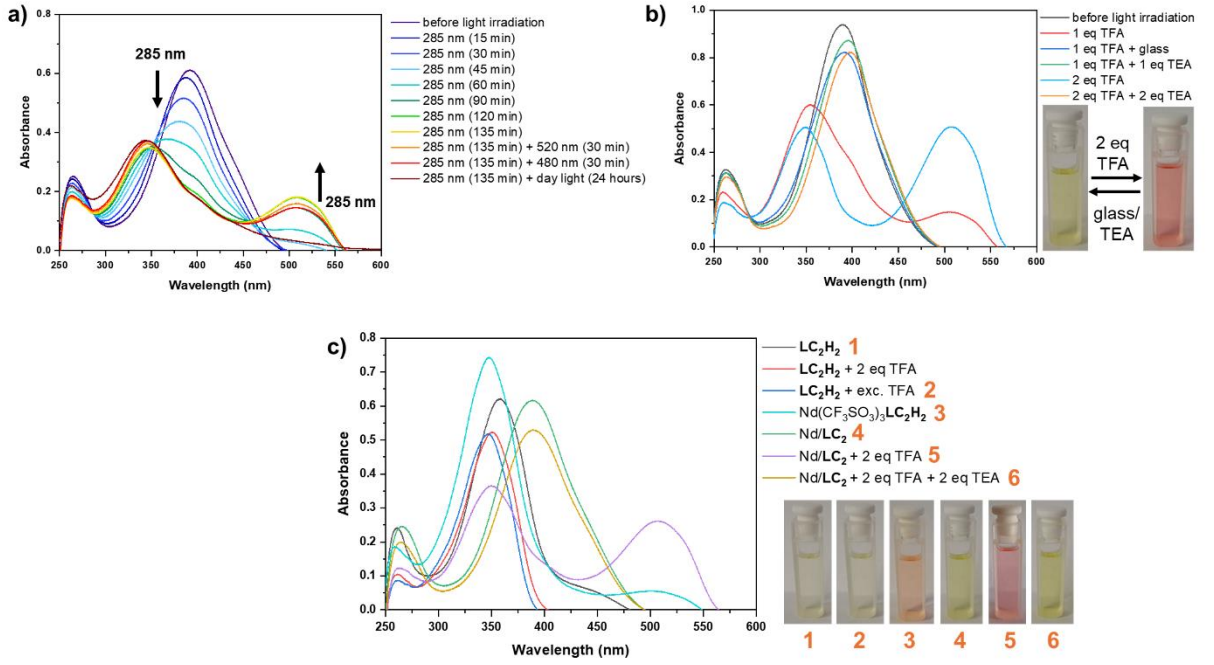

Fig. S42. UV-Vis absorption spectra changes under defined conditions for Nd/**LC_2** lanthanide complex (a), Dy/**LC_2** lanthanide complex (acid-base equilibrium) (b) and **LC_2H_2** ligand with comparison for its deprotonated or not deprotonated Nd^{3+} complexes (c). The photos inserted into the graphs show specific changes in the colour of the solutions.

9. Literature

1. N. T. Coogan, M. A. Chimes, J. Raftery, P. Mocilac and M. A. Denecke, Regioselective Synthesis of V-Shaped Bistriazinyl-phenanthrolines, *J. Org. Chem.*, 2015, **80**, 8684-8693.

2. M. Loos, C. Gerber, F. Corona, J. Hollender and H. Singer, Accelerated Isotope Fine Structure Calculation Using Pruned Transition Trees, *Anal. Chem.*, 2015, **87**, 5738-5744.

3. P. Pracht, F. Bohle and S. Grimme, Automated exploration of the low-energy chemical space with fast quantum chemical methods, *Phys. Chem. Chem. Phys*, 2020, **22**, 7169-7192.

4. G. Forte, A. Grassi and G. Marletta, Molecular Modeling of Oligopeptide Adsorption onto Functionalized Quartz Surfaces, *J. Phys. Chem. B.*, 2007, **111**, 11237-11243.

5. M. J. Frisch, Trucks, G.W., Schlegel, H.B., Scuseria, G.E., Robb, M.A., Cheeseman, J.R., et al. , Gaussian 16 Rev. C.01. Wallingford, CT., 2016.

6. G. Sheldrick, SHELXT - Integrated space-group and crystal-structure determination, *Acta Crystallogr. Sect. A.* , 2015, **71**, 3-8.

7. G. M. Sheldrick, Crystal structure refinement with SHELXL, *Acta Crystallogr. Sect. C-Struct. Chem.*, 2015, **71**, 3-8.

8. A. Spek, PLATON SQUEEZE: a tool for the calculation of the disordered solvent contribution to the calculated structure factors, *cta Crystallogr. Sect. C* 2015, **71**, 9-18.